JCI insight

RESEARCH ARTICLE

NKp46-expressing human gut-resident intraepithelial Vδ1 T cell subpopulation exhibits high antitumor activity against colorectal cancer

Joanna Mikulak,[1,2] Ferdinando Oriolo,[1,2] Elena Bruni,[1,2] Alessandra Roberto,[3] Federico S. Colombo,[4] Anna Villa,[5,6] Marita Bosticardo,[5] Ileana Bortolomai,[5] Elena Lo Presti,[7,8] Serena Meraviglia,[7,8] Francesco Dieli,[7,8] Stefania Vetrano,[9,10] Silvio Danese,[9,10] Silvia Della Bella,[1,2] Michele M. Carvello,[11] Matteo Sacchi,[11] Giovanni Cugini,[12] Giovanni Colombo,[12] Marco Klinger,[2,13] Paola Spaggiari,[14] Massimo Roncalli,[10,11,12,13,14] Immo Prinz,[15] Sarina Ravens,[15] Biagio di Lorenzo,[16,17] Emanuela Marcenaro,[18,19] Bruno Silva-Santos,[16] Antonino Spinelli,[10,11] and Domenico Mavilio[1,2]

[1]Unit of Clinical and Experimental Immunology, Humanitas Clinical and Research Center, Rozzano, Milan, Italy. [2]Department of Medical Biotechnologies and Translational Medicine (BioMeTra), University of Milan, Milan, Italy. [3]Laboratory of Translational Immunology and [4]Humanitas Flow Cytometry Core, Humanitas Clinical and Research Center, Rozzano, Milan, Italy. [5]San Raffaele Telethon Institute for Gene Therapy (SR-TIGET), Division of Regenerative Medicine, Stem Cells and Gene Therapy, San Raffaele Scientific Institute, Milan, Italy. [6]Istituto di Ricerca Genetica e Biomedica, Consiglio Nazionale delle Ricerche, Milan, Italy. [7]Central Laboratory for Advanced Diagnostic and Biomedical Research (CLADIBIOR) and [8]Department of Biopathology and Medical Biotechnologies (DIBIMED), University of Palermo, Palermo, Italy. [9]IBD Center, Laboratory of Gastrointestinal Immunopathology, Humanitas Clinical and Research Center, Rozzano, Milan, Italy. [10]Department of Biomedical Sciences, Humanitas University, Rozzano, Milan, Italy. [11]Colon and Rectal Surgery Unit, [12]Otorhinolaryngology Department, [13]Plastic Surgery Unit, and [14] Department of Pathology, Humanitas Clinical and Research Center, Rozzano, Milan, Italy. [15]Institute of Immunology, Hannover Medical School, Hannover, Germany. [16]Instituto de Medicina Molecular, Faculdade de Medicina, and [17]Instituto Superior Técnico, Universidade de Lisboa, Lisboa, Portugal. [18]Department of Experimental Medicine and [19]Centre of Excellence for Biomedical Research, University of Genoa, Genoa, Italy.

γδ T cells account for a large fraction of human intestinal intraepithelial lymphocytes (IELs) endowed with potent antitumor activities. However, little is known about their origin, phenotype, and clinical relevance in colorectal cancer (CRC). To determine γδ IEL gut specificity, homing, and functions, γδ T cells were purified from human healthy blood, lymph nodes, liver, skin, and intestine, either disease-free, affected by CRC, or generated from thymic precursors. The constitutive expression of NKp46 specifically identifies a subset of cytotoxic Vδ1 T cells representing the largest fraction of gut-resident IELs. The ontogeny and gut-tropism of NKp46$^+$/Vδ1 IELs depends both on distinctive features of Vδ1 thymic precursors and gut-environmental factors. Either the constitutive presence of NKp46 on tissue-resident Vδ1 intestinal IELs or its induced expression on IL-2/IL-15–activated Vδ1 thymocytes are associated with antitumor functions. Higher frequencies of NKp46$^+$/Vδ1 IELs in tumor-free specimens from CRC patients correlate with a lower risk of developing metastatic III/IV disease stages. Additionally, our in vitro settings reproducing CRC tumor microenvironment inhibited the expansion of NKp46$^+$/Vδ1 cells from activated thymic precursors. These results parallel the very low frequencies of NKp46$^+$/Vδ1 IELs able to infiltrate CRC, thus providing insights to either follow-up cancer progression or to develop adoptive cellular therapies.

Authorship note: JM and FO contributed equally to this work.

Conflict of interest: BSS is a cofounder and shareholder of Lymphact – Lymphocyte Activation Technologies S.A.

Submitted: October 29, 2018
Accepted: October 31, 2019
Published: November 5, 2019.

Reference information: *JCI Insight*. 2019;4(24):e125884. https://doi.org/10.1172/jci.insight.125884.

Introduction

The gastrointestinal (GI) tract is considered the largest immunological organ in the human body with both circulating and tissue-specific immune cells either organized in several structures of the lamina propria (LP) or resident within the epithelium. The synergic interactions of immune cells with both epithelial cells and microbiota shape innate and adaptive immune responses, set up the threshold between immune tolerance and effector functions, and also balance the efficacy of checkpoint blockade in cancer immunotherapy (1, 2).

The human gut epithelium is home to large numbers of T cells expressing γδ T cell receptors (TCR), which account for the main fraction of all intraepithelial lymphocytes (IELs) (3). While the exact functions of γδ IELs remain elusive, they have been suggested to control antimicrobial defense, organ homeostasis, and tissue damage repair (4, 5). Indeed, γδ T cell–deficient mice present abnormalities in gut epithelial morphology, reduced MHC-II expression by enterocytes, and impaired mucosal IgA production (6, 7). Although γδ T cells originate from common thymic precursors alongside αβ T cells, they are considered innate-like lymphocytes for their rapid and non-MHC–restricted effector responses such as cytotoxicity and secretion of type I cytokines (8). Human γδ T cells are broadly divided into 2 main Vδ1 and Vδ2 subsets based on their TCRδ chain repertoire (9). Under homeostatic conditions, Vδ2 cells are mainly enriched in peripheral blood, where they represent about 5% of all circulating T cells and recognize specifically microbial or stress- or tumor-induced phosphoantigens (8, 10–12). In contrast, Vδ1 cells are preferentially localized in peripheral tissues such as the gut, skin, and liver. However, very little is known about their organ specificity and local antigen/ligand recognition.

Growing evidence confirmed the important role of γδ T lymphocytes in tumor immune surveillance and provided promising perspectives in cancer immunotherapy (13). Indeed, both Vδ1 and Vδ2 subsets expanded from peripheral blood are endowed with high antitumor activities against hematological malignances and solid tumors in vivo and in vitro (14). Therefore, much effort has been made to improve blood γδ T cell–mediated tumor recognition and killing (15). In this context, we previously showed that the TCR stimulation in vitro induces a de novo expression of natural cytotoxic receptors (NCRs) (mainly NKp30) on circulating Vδ1 T cells, thus remarkably increasing their antitumor effector functions (16). Therefore, NCRs are no longer considered as specific NK cell activating receptors (aNKR) and are currently being implemented for developing adoptive cellular therapies against cancers (17, 18).

In contrast to the peripheral blood γδ T cells that have received much attention, both phenotype and antitumor potentials, as well as the mechanisms regulating the homeostasis of human tissue-resident γδ T cells, are still largely unknown. Indeed, while mice share some common innate-like functions of human γδ T cells, they differ significantly in terms of TCR specificity and tissue specialization (19). Nonetheless, several studies reported that, in different types of human cancers, including colorectal cancer (CRC), high frequencies of intratumoral γδ T cells represent one of most favorable prognostic markers in tumor clinical outcomes (20, 21). Therefore, there is a pressing need to better characterize human tissue-resident γδ T lymphocytes in order to understand their impact in the physiopathology of cancer.

The present study identifies a subset of gut-resident Vδ1 IELs naturally expressing high levels of NKp46. The presence of this NCR characterizes the largest subset of γδ T cells among intestinal IELs, a population that we could not detect in healthy human skin, lymph nodes, or liver; we also could not detect it in the gut of WT mice strains. NKp46$^+$/Vδ1 IELs share the same phenotypic and antitumor effector functions of NKp46$^+$/Vδ1 T cells generated from thymic precursors following activation with IL-2 or IL-15, 2 cytokines highly enriched in gut microenvironment that confer to Vδ1 thymocytes a specific gut tropism. Low frequencies of the NKp46$^+$/Vδ1 IEL subset in healthy gut specimens of patients affected by CRC are associated with a faster tumor progression and development of metastatic diseases, thus suggesting a protective role and a potential prognostic value of these tissue-resident innate-like lymphocytes in CRC.

Results

Identification of a subset of NKp46$^+$ γδ intestinal intraepithelial T lymphocytes. Human healthy colon specimens obtained from patients who underwent surgical resection for CRC were located at the distal part (≥10 cm in length) of the removed tumor core and were considered "tumor-free/healthy" after a conventional macroscopic and microscopic examination by pathologists. Healthy gut specimens were processed to obtain IELs and LP lymphocytes (LPLs) (Supplemental Figure 1, A–C; supplemental material available online with this article; https://doi.org/10.1172/jci.insight.125884DS1). As expected (22), the frequency of γδ T cells appeared to be significantly higher among IELs compared with both LPLs and peripheral blood mononuclear cells (PBMCs) (Figure 1, A and B). Unlike circulating γδ T cells, both γδ IELs and LPLs presented high levels of the tissue-resident marker CD69 (23). The different location of intestinal γδ IELs and LPLs was also confirmed by specific high expression on the first subset, and not on the second one, of CD103, the main adhesion molecule involved in the specific retention of IELs in the epithelial layer (Figure 1C and ref. 24). We also observed that γδ IELs are characterized by significantly higher expression of CD56 and CD8 compared with γδ LPLs, while expressing low surface levels of CD4. These phenotypic features of γδ

IELs are also associated with low amounts of inhibitory NKRs (iNKRs) (e.g., NKG2A and KIRs) and high expression of aNKRs (e.g., NKG2C and NKG2D), thus suggesting that γδ IELs are endowed with a high cytolytic potential (Figure 1D).

Circulating γδ T cells do not physiologically express NCRs (16). In contrast, we found that γδ IELs constitutively express high levels of NKp46, while their counterparts from LP showed a significantly lower natural expression of this NCR. Although at a minor extent compared with NKp46, γδ IELs are also NKp44$^+$ in contrast to γδ LPLs and PBMCs that have significantly lower surface levels of this NCR. No significant differences were observed for NKp30 surface levels between γδ T intestinal cells (both IELs and LPLs) and PBMCs (Figure 1E and Supplemental Figure 1D). The presence of NKp46$^+$ γδ T cells in the intraepithelial (IE) compartment of human intestine was also confirmed by confocal microscopy (Supplemental Figure 1E).

CD8$^+$ γδ IELs had been first characterized as a subset of unconventional T cells expressing, in their TCR complex, the homodimer CD8αα, which induces cell hyporesponsiveness/anergy (25). Another study later identified a population of high cytotoxic and immune-regulatory intestinal CD8$^+$ γδ T cells carrying the heterodimer CD8αβ. This latter immunoregulatory subset plays a key role in the homeostasis of gut-associated lymphoid tissue and in the pathogenesis of inflammatory bowel disease (IBD) (26). Our results showed that, while the entire population of CD8$^+$ γδ IELs express significantly higher levels of α rather than β chain, the subset of NKp46$^+$/CD8$^+$ γδ IELs coexpresses similar levels of α and β chains in their CD8 receptor (Figure 1F).

CD45$^+$/CD3$^+$ IELs from healthy gut specimens were also analyzed by a dimensionality reduction method that used the t-distributed stochastic neighbor embedding (t-SNE) algorithm. Two different and separate clusters of NKp46$^-$ (C1) NKp46$^+$ (C2) γδ IELs were identified on the basis of population boundaries distinguishable on the polychromatic flow cytometry density plots (Figure 1G). The related heatmap showed that C1 and C2 are characterized by distinctive phenotypes with higher expression of NKp44, NKp30, CD8β, CD56, NKG2C, and NKG2D and lower expression of inhibitory killer immunoglobin receptors (KIRs) in NKp46$^+$ γδ IELs compared with NKp46$^-$ γδ IELs (Figure 1H).

Taken together, this first set of data indicates that the presence of NKp46 identifies a specific cluster of intestinal CD8 γδ IELs carrying the heterodimer CD8αβ and whose phenotype is likely associated with immune effector functions (e.g., cytotoxicity and cytokine production) rather than immune tolerance.

NKp46$^+$ γδ IELs are Vδ1 restricted and preferentially enriched in human intestine. As expected (25), γδ IELs comprised higher proportions of Vδ1 T cells in contrast to their counterpart in the blood, known to be mainly Vδ2 restricted (8). A consistent fraction of γδ LPLs neither express Vδ1 nor Vδ2 chain, a phenomenon that we also observed within both IEL and PBMC compartments, although at a lower extent (Figure 2A). Therefore, the intestinal LP compartment might be, together with human liver, another preferential tissue where other γδ T cell subsets, such as the Vδ3$^+$ subset, could reside (27). Interestingly, we found that NKp46 specifically identifies Vδ1 IELs, while Vδ2 IELs express significantly lower amounts of this NCR. NKp44 marks only a small fraction of γδ IELs, with the Vδ1 subset expressing significantly higher levels of this NCR compared with the Vδ2 population. Both Vδ1 and Vδ2 IELs express very low levels of NKp30 (Figure 2, B and C).

Vδ1 IELs are characterized by a CD4$^-$/CD8$^+$ phenotype with high surface levels of CD56 and NKG2D, while expressing low amounts of NKG2A and KIRs. In contrast, Vδ2 IELs express significantly lower levels of CD8 and CD56 together with significantly higher amounts of NKG2A when compared with their Vδ1 counterpart (Figure 2D). We then purified IELs from matched healthy ileum and colon specimens from patients affected by Crohn's disease and having undergone surgical gut resection. We found similar frequencies of Vδ1 and Vδ2 T IELs both in ileum and colon, with a higher percentage of Vδ1 compared with Vδ2 cells (Supplemental Figure 2A). Again, the NKp46 expression in the ileum is mainly restricted on Vδ1 IELs in both anatomical sites without any statistically significant differences between ileum and colon (Supplemental Figure 2B). These results indicate that NKp46$^+$/Vδ1 lymphocytes represent the largest and most ubiquitous γδ T cell population within the IEL compartment of both small and large intestine.

We then determined the constitutive NCR expression on γδ T cells purified from other human healthy tissues known to be highly enriched of these innate-like T cells: skin, liver, and lymph nodes (5, 28). Although skin and liver are predominantly enriched with the Vδ1 cell subset over the Vδ2 subset, they do not express NCRs in both tissue sites. Similarly, also Vδ1 and Vδ2 T cells purified from lymph nodes are NKp46$^-$ and NKp44$^-$, while a minor fraction of both subsets is NKp30$^+$ (Supplemental Figure 3).

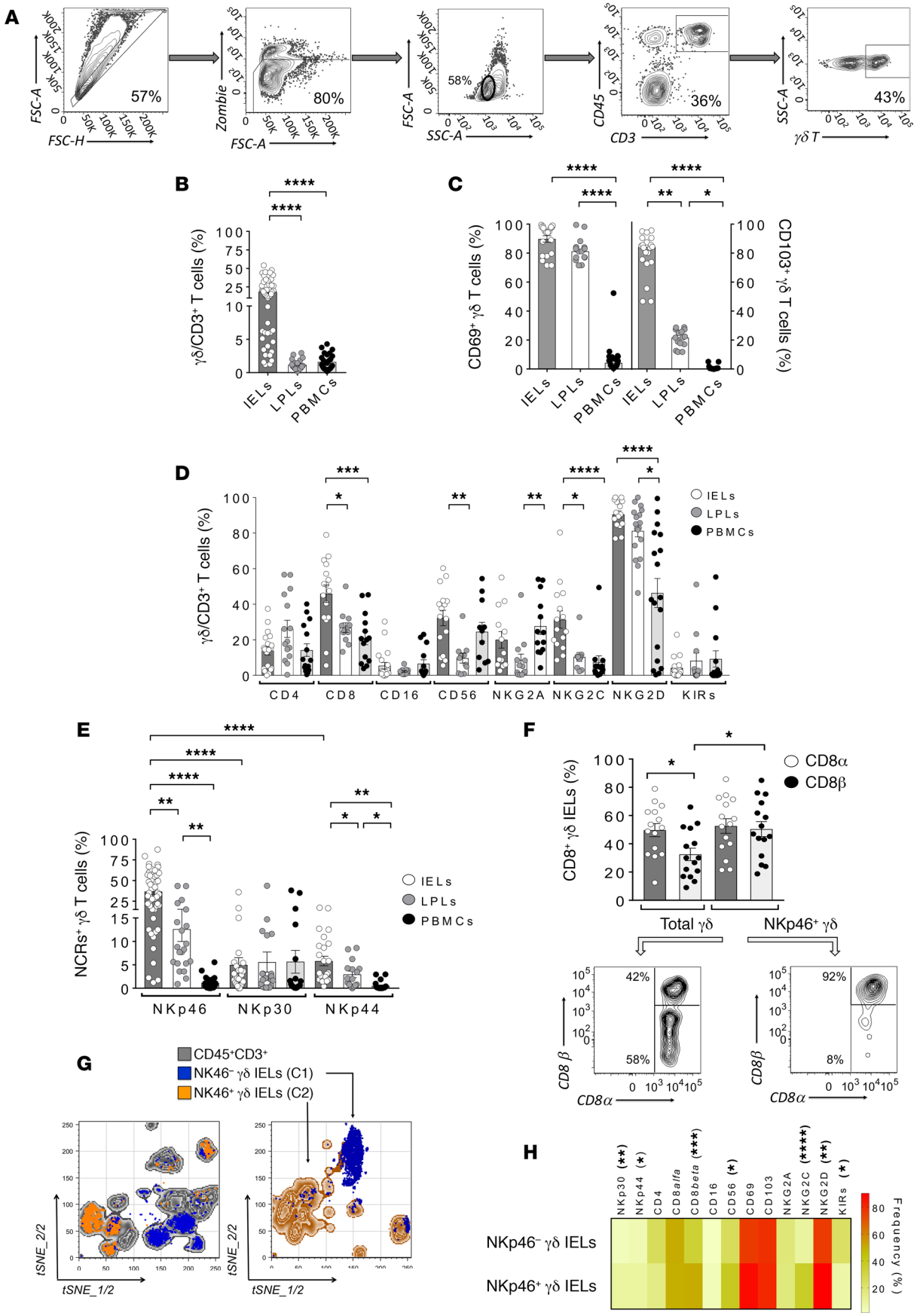
A
FSC-A
FSC-H
57%
Zombie
FSC-A
80%
FSC-A
SSC-A
58%
CD45
CD3
36%
SSC-A
γδ T
43%
B
γδ/CD3⁺ T cells (%)
IELs
LPLs
PBMCs
C
CD69⁺ γδ T cells (%)
CD103⁺ γδ T cells (%)
IELs
LPLs
PBMCs
D
γδ/CD3⁺ T cells (%)
IELs
LPLs
PBMCs
CD4
CD8
CD16
CD56
NKG2A
NKG2C
NKG2D
KIRs
E
NCRs⁺ γδ T cells (%)
IELs
LPLs
PBMCs
NKp46
NKp30
NKp44
F
CD8⁺ γδ IELs (%)
CD8α
CD8β
Total γδ
NKp46⁺ γδ
42%
58%
92%
8%
CD8β
CD8α
G
CD45⁺CD3⁺
NK46⁻ γδ IELs (C1)
NK46⁺ γδ IELs (C2)
tSNE_2/2
tSNE_1/2
H
NKp30 (**)
NKp44 (*)
CD4
CD8alfa
CD8beta (***)
CD16
CD56 (*)
CD69
CD103
NKG2A
NKG2C (****)
NKG2D (**)
KIRs (*)
NKp46⁻ γδ IELs
NKp46⁺ γδ IELs
Frequency (%)

Figure 1. Identification of a subset of NKp46⁺ intraepithelial Vδ1 T lymphocytes highly enriched in human healthy intestine. (**A**) Representative example of flow cytometry dot plots showing the gating strategy used to identify viable CD45⁺/CD3⁺ γδ T lymphocyte both in intraepithelial (IEL) and lamina propria (LPL) compartments from specimens of human healthy colon. (**B**) Summary statistical graph showing within the CD45⁺/CD3⁺ lymphocytes the percentages of γδ IELs (n = 54 in white circles), γδ LPLs (n = 20 in gray circles) from human healthy colon specimens, and γδ peripheral blood mononuclear cells (PBMCs) (n = 26 in black circles) of healthy donors. (**C**) Summary statistical graph showing the expression percentage of CD69 and CD103 on γδ IELs (n = 20 in white circles), γδ LPLs (n = 15 in grey circles) from specimens of human healthy colon, and on γδ T cell from PBMCs (n = 20 in black circles) of healthy donors. (**D**) Summary statistical graph showing the expression percent of CD4, CD8, CD16, CD56, NKG2A, NKG2C, NKG2D, and killer immunoglobulin-like receptors (KIRs) on γδ IELs ($n \geq 13$, white circles), γδ LPLs ($n \geq 10$ in gray circles) from specimens of human healthy colon, and on γδ T cells from PBMCs of healthy donors ($n \geq 13$, black circles). (**E**) Summary statistical graph showing the expression percent of NKp46, NKp30, and NKp44 on γδ IELs ($n \geq 25$ in white circles), γδ LPLs ($n \geq 16$ in gray circles) from specimens of human healthy colon, and on γδ T cells from PBMCs from healthy donors ($n \geq 25$ in black circles). (**F**) Summary statistical analysis (upper graph) showing the expression of CD8α (white circles) and CD8β (black circles) chains within the CD8 receptor of matched CD8⁺ γδ IELs and CD8⁺/NKp46⁺ γδ IELs from specimens of human healthy colon (n = 15). White arrows indicate representative flow cytometry dot plots showing coexpression of CD8α and CD8β chains in CD8⁺ total γδ T (left) or NKp46⁺/γδ T IELs (right), respectively. (**G**) t-SNE graphs from a representative specimen of human healthy colon showing the clustering of NKp46⁻ (C1 in blue) and NKp46⁺ (C2 in orange) γδ IELs within CD45⁺/CD3⁺ lymphocytes (gray; left panel) or in γδ T IELs (right panel). (**H**) Heatmap graph showing the degree of expression of several surface markers on matched NKp46⁻ and NKp46⁺ γδ IEL clusters defined as C1 and C2 in panel **G** (n = 7). *$P \leq 0.05$; **$P \leq 0.01$; ***$P \leq 0.001$; ****$P \leq 0.0001$.

Even though murine and human γδ T cells differ in several phenotypic features and tissue distribution, Vδ1 T cells have been shown to be more similar between the 2 species compared with their Vδ2 counterparts (19). Moreover, NKp46 is the only NCR to be phylogenetically conserved in mice and humans (29). Therefore, we investigated whether human NKp46⁺/Vδ1 IELs have an equivalent in the intestine of BALB/c and C57BL/6 mice strains. Although murine gut contains high frequencies of γδ T IELs, they do not express NKp46. Instead, tissue-resident NK cells from the same murine specimens express, as expected, detectable levels of this NCR and were used as internal positive controls of these experiments in mice (Supplemental Table 1 and Supplemental Figure 4). We also found that the degree of frequency of total γδ IELs and NKp46⁺/Vδ1 IELs in the intestine is independent of both age and sex (Supplemental Figure 5).

Common features but distinct TCR repertoire of NKp46⁺ and NKp46⁻ IEL subsets. The repertoire of γδ TCR was analyzed via high-throughput sequencing of V(D)J regions of either the γ chain (TRG) or δ chain (TRD) expressed on FACS-sorted Vδ1 NKp46⁺ and NKp46⁻ IELs. The purity of all sorted samples was ≥ 95% (Supplemental Figure 6). Our data showed that the TRG repertoires of total NKp46⁺ and NKp46⁻ Vδ1 IELs is mainly represented by highly expanded Vγ9⁻ γδ T cell clones (Figure 3A). We also observed more recurrent usage of Vγ4⁺ sequences in the NKp46⁺ IEL subset among different individuals (Figure 3B). On the other hand, extended variability of Vγ chains with similar incidence of Vγ9⁺ and Vγ4⁺ sequences were presented in NKp46⁻ IELs. For TRD repertoires, we found a considerable fraction of Vδ2⁺ sequences within Vδ1 IELs (data not shown), a phenomenon highly similar to what was recently observed in human Vδ1 γδ thymocytes (30). We then focused our analyses only on Vδ1⁺ IELs, and the results showed that the sequences of NKp46⁺ and NKp46⁻ γδ subsets were characterized by highly clonal TRD repertoires; the majority of Vδ1 TRD clones used the Jδ1-joining element (Figure 3C). Notably, the overall TCR repertoire diversity is largely similar between NKp46⁺ and NKp46⁻ IELs (Figure 3D). The number of shared TRG and TRD clones, calculated between all samples, shows only a few overlapping clones within the γδ IEL compartment, mainly Vγ4⁺ or Vγ9⁺ (Figure E). Importantly, the most expanded TRG and TRD clones do not overlap between NKp46⁺ and NKp46⁻ γδ IELs within the same individual (Figure 3, A, C, and E). Taken together, the predominant individual clonal TRD and TDG repertoires of NKp46⁺ and NKp46⁻ IEL subsets and the lack of overlapping clones between NKp46⁺ and NKp46⁻ γδ IELs suggest that these 2 IEL subsets emerge from distinct Vδ1 T cell progenitors.

NKp46 expression on γδ IELs is associated with high cytolytic potential and production of IFN-γ. Cytokines such as IL-10, IL-17, IL-22, and TGF-β play important roles in regulating intestinal immune system homeostasis and are highly enriched in the gut mucosa microenvironment (31). In addition, studies have shown that freshly isolated and activated γδ IELs express high levels of lymphotactin/XCL1, a chemokine important for CD8⁺ T cell activity and chemotaxis (32). Therefore, we compared the transcription levels of these cytokines between circulating γδ T cells and fresh FACS-sorted NKp46⁺ and NKp46⁻ γδ IELs. Our results showed that both NKp46⁺ and NKp46⁻ γδ IELs express similarly high mRNA amounts of IL-22 and lymphotactin/XCL1 compared with blood γδ T cells, thus highlighting their key roles in IE immune responses and homeostasis. No differences were found for IL-10, IL-17, and TGF-β transcripts between NKp46⁺ and NKp46⁻ γδ IELs and circulating γδ T cells (Figure 4A).

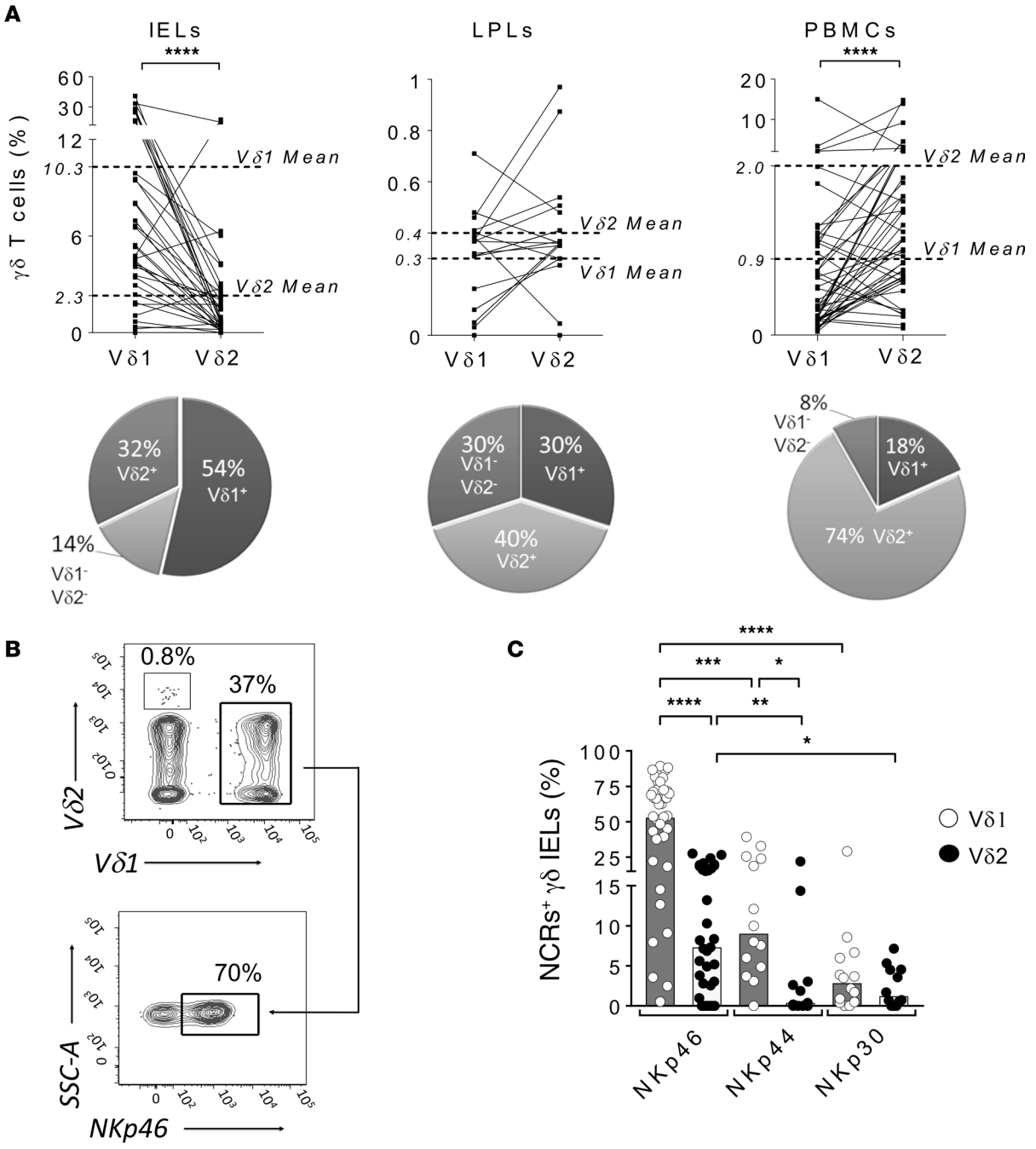
A
IELs
LPLs
PBMCs
****
γδ T cells (%)
Vδ1 Mean
Vδ2 Mean
Vδ1
Vδ2
32% Vδ2+
54% Vδ1+
14% Vδ1- Vδ2-
30% Vδ1- Vδ2-
30% Vδ1+
40% Vδ2+
8% Vδ1- Vδ2-
18% Vδ1+
74% Vδ2+
B
0.8%
37%
70%
Vδ2
Vδ1
SSC-A
NKp46
C
NCRs+ γδ IELs (%)
Vδ1
Vδ2
NKp46
NKp44
NKp30
D
γδ IELs (%)
CD4
CD8
CD16
CD56
NKG2A
NKG2D
KIRs

Figure 2. NKp46$^+$ γδ IELs are Vδ1 restricted and express a cytotoxic phenotype. (**A**) Summary statistical graphs (upper line) showing, within the entire CD45$^+$/CD3$^+$ lymphocyte population, the percentages of Vδ1 or Vδ2 IEL (n = 37) and LPL ($n \geq 22$) subsets from specimens of human healthy colon and from PBMCs (n = 49) of healthy donors. Data are represented as scattered plots of paired observations. Pie charts showing the percentages of Vδ1$^+$, Vδ2$^+$, and Vδ1$^-$/Vδ2$^-$ subsets within total γδ T cells of matched samples (n = 10) of IELs and LPLs from specimens of human healthy colon and PBMCs of healthy donors. (**B**) Representative examples (out of 38) of contour plots showing the percentages of Vδ1$^+$ and Vδ2$^+$ T cell subset (upper panel) and of NKp46$^+$/Vδ1 T cells (lower panel) within total purified γδ IELs from a specimen of human healthy colon. (**C**) Summary statistical graph showing the frequencies of Vδ1 (white circles) and Vδ2 (black circles) IELs ($n \geq 20$) from specimens of human healthy colon expressing NKp46, NKp44, and NKp30. (**D**) Summary statistical graph showing the frequencies of Vδ1 (white circles) and Vδ2 (black circles) IELs ($n \geq 16$) from specimens of human healthy colon expressing CD4, CD8, CD16, CD56, NKG2A, NKG2D, and KIRs. *$P \leq 0.05$; **$P \leq 0.01$; ***$P \leq 0.001$; ****$P \leq 0.0001$.

We then analyzed their IFN-γ production and cytolytic potential after coculture with K562 cells, a tumor target widely employed to test innate cell cytotoxicity (33). NKp46$^+$ and γδ IELs showed a significantly increased production of IFN-γ in response to the K562 cells compared with their NKp46$^-$ counterparts (Figure 4B). We then observed that the intracellular level of Granzyme B (GZMB) is constitutively higher in freshly purified NKp46$^+$ γδ IELs compared with their NKp46$^-$ counterparts. The incubation with K562 cells further increased the amount of newly synthesized intracellular GZMB both in NKp46$^+$ and NKp46$^-$ γδ IELs. However, the amounts of this cytotoxic granule were significantly higher in the first subset compared with the second one (Figure 4C). We then measured the degree of CD107a expression as a marker of cytolytic activity. Again, the frequencies of CD107a$^+$/NKp46$^+$ γδ IELs were significantly higher compared with those of CD107a$^+$/NKp46$^-$ γδ IELs following incubation with K562 (Figure 4D). Additional experiments also confirmed the great cytotoxic potential of NKp46$^+$ γδ IELs in killing human colon adenocarcinoma cell targets (e.g., SKCO1 and Caco2) (Figure 4E).

To assess the functional relevance of NKp46 in the highly cytotoxic potentials of NKp46$^+$ γδ IELs, we tested the ability of these cells to degranulate either in the presence or in the absence of the specific anti-NKp46 mAb. The results showed that the masking of NKp46 significantly decreases the ability of NKp46$^+$ γδ IELs to kill K562 (Figure 4F), thus demonstrating a direct involvement of this aNKR in tuning the cytotoxicity of this specific epithelial γδ T cell subset.

Human γδ thymocytes resemble the phenotype and functions of NKp46$^+$ Vδ1 IELs following activation. Maturation of γδ T cells occurs during thymus development that commits γδ T precursors to properly differentiate and migrate to peripheral tissues (34). Recently, it has been also reported that the acquisition of both cytotoxicity and ability to produce IFN-γ by γδ thymic precursors is not associated with the engagement of TCR, but rather requires activation with either IL-2 or IL-15 (35). In order to understand whether these 2 cytokines could induce phenotype and functions similar to those of NKp46$^+$ Vδ1 IELs at the level of γδ thymic precursors, we stimulated, with both these cytokines, γδ thymocytes purified from healthy thymus collected from pediatric patients undergoing cardiac surgical procedures. The activation with either IL-2 or IL-15 induced a statistically significant increase of NKp46, while this was not the case for γδ thymocytes incubated with IL-7 (Figure 5A). Interestingly, the activation with IL-2 induced a preferential expansion of the NKp46$^+$/Vδ1 T cell subset, as we did not detect any significant proliferation within the Vδ2 cell compartment (Figure 5, B and C). The expansion of Vδ1 thymocytes was mainly associated with an increased de novo expression of NKp46, as we observed very few NKp46$^+$/Vδ1 cells in freshly isolated thymocytes (data not shown). We also found that IL-2 activation induces a de novo expression of NKp46 on FACS-sorted Vδ1 thymocytes and not on their Vδ2 FACS-sorted counterparts, thus indicating the intrinsic ability of this cytokine to generate NKp46$^+$/Vδ1 T cells from their thymic Vδ1 precursors without the need of additional cellular interactions (data not shown).

Activation with IL-2 induces, on γδ thymocytes, a significant de novo expression of NKp44 and NKp30 receptors, although to a lesser extent compared with that of NKp46. In contrast, we did not detect any induced expression of NCRs on αβ thymocytes or peripheral γδ T cells following incubation with IL-2 (Figure 5D). Similar results were observed with IL-15 (data not shown).

Interestingly, the phenotype of Vδ1 cells expanded from IL-2–activated γδ thymic precursors resembled the phenotype of NKp46$^+$/Vδ1 IELs freshly purified from human intestine. Indeed, the incubation with IL-2 (and with IL-15, as well; data not shown) increased on proliferating Vδ1 thymocytes the expression of CD8, CD56, and NKG2D ,while decreasing the surface levels of CD4. Only NKG2A was differently expressed on Vδ1$^+$ cells generated from IL-2 activated thymic precursors compared with freshly purified intestinal NKp46$^+$/Vδ1 IELs. Indeed, while this latter subset naturally expresses very

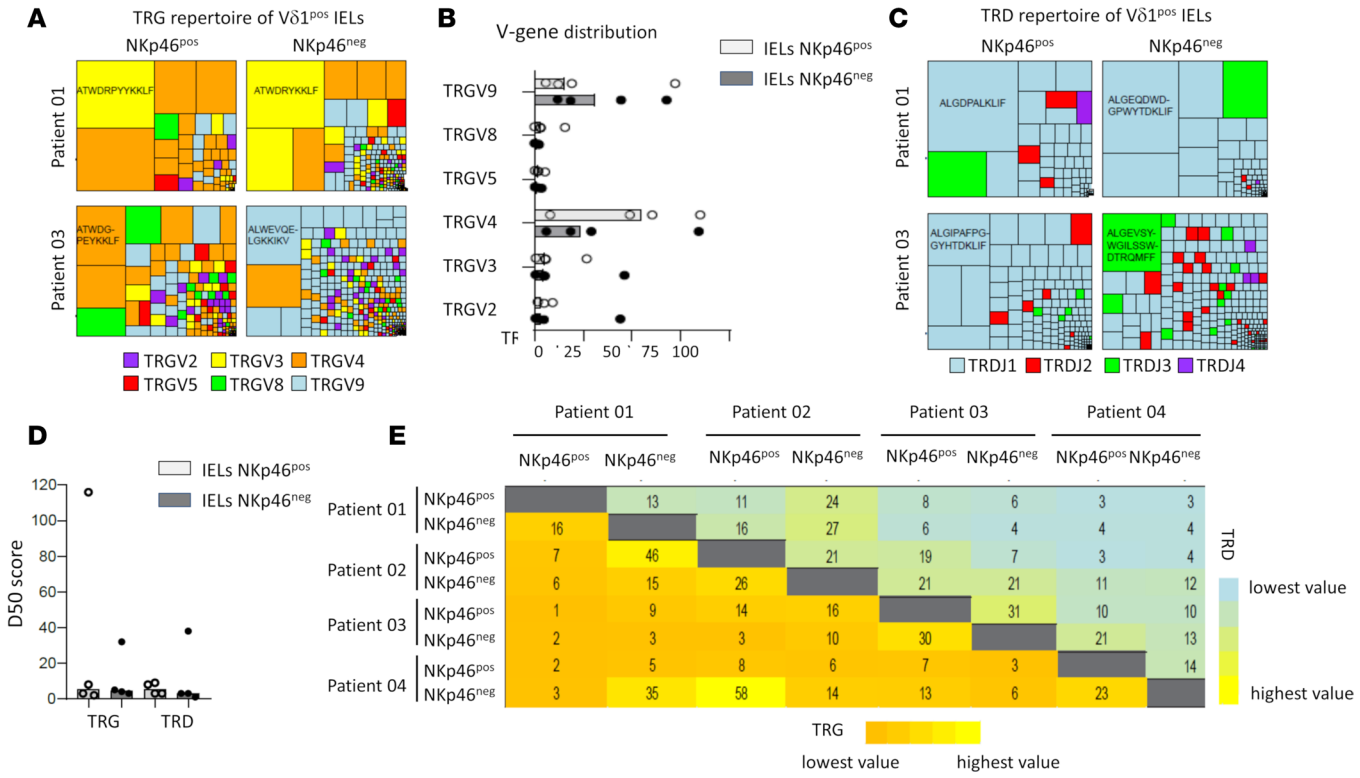

Figure 3. TCR repertoires of NKp46⁺ and NKp46⁻ γδ IELs. (**A**) Treemap graphs showing the distribution of TRG clones within NKp46⁺ and NKp46⁻ γδ IELs from 2 representative patients (out of 4). Squares represent individual clones and are proportional to the abundance of the given clone within the TCR repertoire. Color codes indicate V chain usage. CDR3 sequences of the most expanded clones are given. (**B**) Dot plot graph showing the quantification of V chains for TRG repertoires. Each dot represents 1 patient. (**C**) Treemap graphs showing the distribution of Vδ1⁺ TRD clones within NKp46⁺ and NKp46⁻ IELs of 2 patients. Each square indicates 1 clone within the given TRD repertoires. J elements are color coded, and CDR3 sequences of the most expanded clones are indicated. (**D**) Dot plot graph showing the TRG and TRD diversity that is determined by the D50 score (number of clones within 50% of the given TCR repertoire). Each dot represents 1 patient. (**E**) Heatmap graph displaying the number of shared TRG (lower part, orange–yellow) and TRD (upper part, blue–yellow) clones between patient samples.

low levels of this iNKR, the stimulation of thymic precursors with IL-2 induced a remarkably high de novo expression of NKG2A on Vδ1⁺ thymocytes. The IL-2 stimulation also triggered a de novo expression on Vδ1⁺ cells of CCR9, a chemokine receptor involved in the homing of γδ T lymphocytes to the gut mucosa (Figure 6A and ref. 36). This phenomenon is also functionally relevant, as demonstrated by the chemotactic activity of CCR9 on IL-2–activated NKp46⁺/Vδ1 thymocytes in response to its CCL25 ligand in a dose-dependent manner (Figure 6B). The acquisition of the NKp46 phenotype on γδ thymocytes following incubation with IL-2 is coupled with significantly higher transcription levels of GZMB, as well as with an increased degranulation against K562 and human tumor epithelial colorectal Caco2 cell lines (Figure 6, C and D).

Taken together, these data indicate that IL-2/IL-15–mediated differentiation of human Vδ1 thymic precursors results in the acquisition of the gut-like phenotype and potent antitumor activity by these cells, which might be committed to specifically migrate to the gut.

Impact of intestinal microenvironment in the maturation of IL-2–activated γδ thymocytes. The preferential enrichment of NKp46⁺/Vδ1 T cells in the intestinal epithelium implicates a tight interaction with intestinal epithelial cells (IECs). Indeed, the survival and the retention of IELs depends on the ligand-activated transcription factor aryl hydrocarbon receptor (AHR) and IL-15 production by neighboring IECs (37). Therefore, we incubated γδ thymocytes with IL-2 in the presence or absence of either primary human colonic epithelial cells (HCoEpic) or IL-15. Both these factors had a significant synergistic effect in further increasing the expression of NKp46 on IL-2–activated Vδ1 proliferating thymocytes (Figure 6E). In contrast, we did not observe any change in NKp46 expression on IL-2–activated thymocytes cocultured with IL-10, IL-12, IL-22, or thymic stromal lymphopoietin (TSLP), the soluble factor produced by IECs to induce T cell maturation at this tissue site (38) (data not shown).

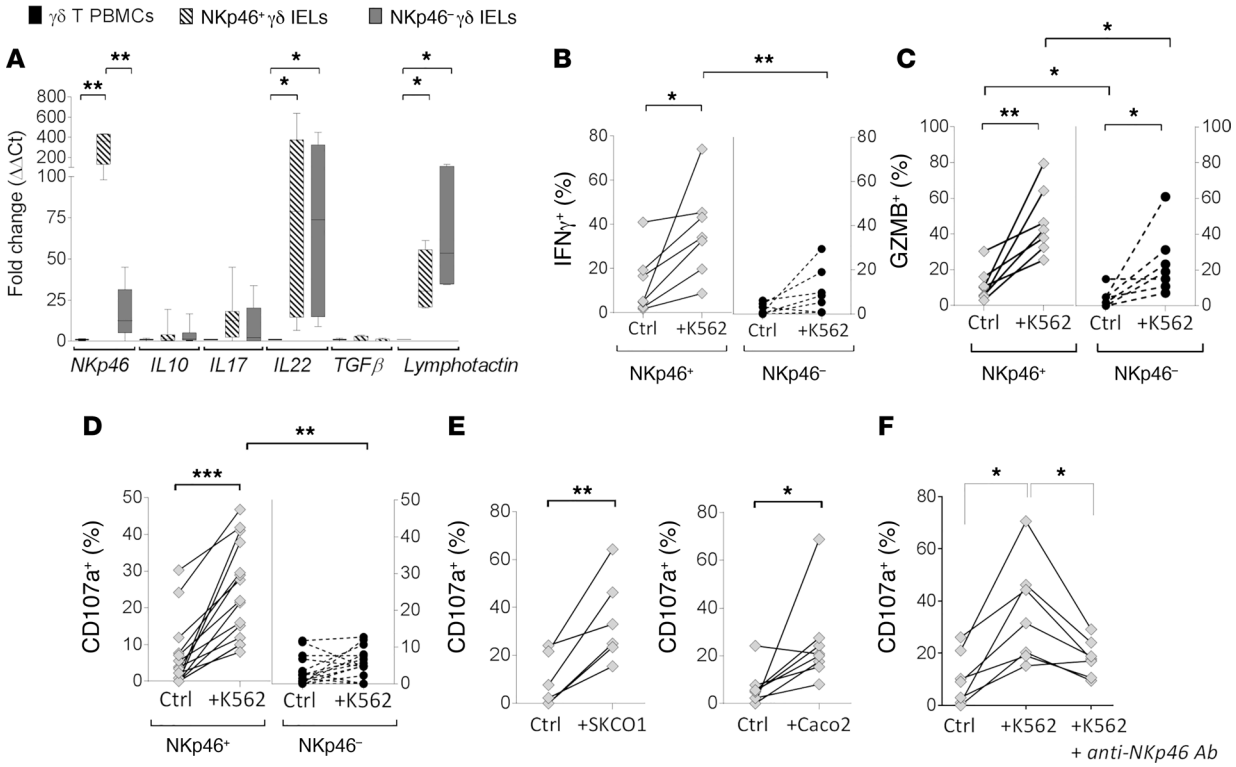

Figure 4. Effector functions of NKp46⁺ γδ IELs. (**A**) Summary statistical graphs showing the transcript levels of NKp46, IL-10, IL-17, IL-22, TGF-β, and lymphotactin/XCL1 and in FACS-sorted NKp46⁺ and NKp46⁻ γδ IELs from specimens of human healthy colon (n = 6) and in FACS-sorted γδ T cell from PBMCs of healthy donors (n = 6). Results are presented as fold changes ($2^{-\Delta\Delta CT}$) of target gene relative to PBMC samples and normalized to housekeeping genes GAPDH and S18. (**B**–**D**) Summary statistical graphs showing the intracellular levels of IFN-γ (**B**), Granzyme B (GMZB) (**C**), and surface expression of CD107a (**D**) by NKp46⁺ and NKp46⁻ γδ IELs from specimens of human healthy colon either in the absence (Ctrl) or in the presence of K562 cell lines. (**E**) Summary statistical graphs showing the surface expression of CD107a by NKp46⁺ γδ IELs from healthy colon either alone or in coculture with tumor target cells SKCO1 (left) and Caco2 (right). (**F**) Summary statistical graph showing the surface expression of CD107a by NKp46⁺ γδ IELs from healthy colon after coculture with K562 either in the absence or presence of a blocking anti–NKp46 IgM mAb (n = 7). *P ≤ 0.05; **P ≤ 0.01; ***P ≤ 0.001.

We also analyzed the contribution of TGF-β that is overexpressed in CRC with poor prognosis, where this protein plays a key role in the organization of tumor microenvironment (39). The incubation with TGF-β significantly suppressed the IL-2–induced expression of NKp46 on proliferating γδ thymocytes. Similar inhibitory results were obtained when IL-2–stimulated γδ thymocytes were cocultured with Caco2 cells (Figure 6E), thus confirming that the intestinal tumor microenvironment is endowed with escape mechanisms impairing the cytolytic potential of Vδ1 T cells.

Impact of NKp46⁺/Vδ1 IELs on the prognosis and progression of CRC. We then assessed if the frequency of γδ IELs in the "disease-free/healthy" tissue specimens of patients affected by CRC correlated with tumor progression. To this end, patients included in the analysis were divided into 2 subcohorts either in early (I/II) or late (III/IV) tumor-nodes metastasis (TNM) stages of CRC on the basis of the widely used TNM staging system. Patients who required chemotherapy treatment before surgical resection of CRC were excluded from the analyses to avoid any bias on T lymphocytes recurrence. We first observed that the frequencies of total γδ IELs, as well as of their Vδ1 and Vδ2 subsets, did not change in the portions of healthy colon from CRC patients at different TNM disease stages (Figure 7, A and B). Interestingly, we found that tumor-free gut specimens of CRC patients that progressed toward stages III/IV had a significantly lower frequency of NKp46⁺/Vδ1 IELs compared with those at earlier I/II stages. This phenomenon appeared to be specific for NKp46⁺/Vδ1 IELs, since no changes in the frequencies of NKp46⁺/Vδ2 IELs were found between I/II and III/IV CRC stages (Figure 7, C and D).

We then evaluated the ability of the NKp46⁺/Vδ1 subset to infiltrate CRC tumor mass. Since this adenocarcinoma originates directly from tumor-transformed IECs and typically disrupts the anatomical organization of gut mucosa in epithelial and LP compartments (Supplemental Figure 1B and ref. 21), we measured the frequency of tumor infiltrating lymphocytes (TILs) on the entire pathologic specimens without

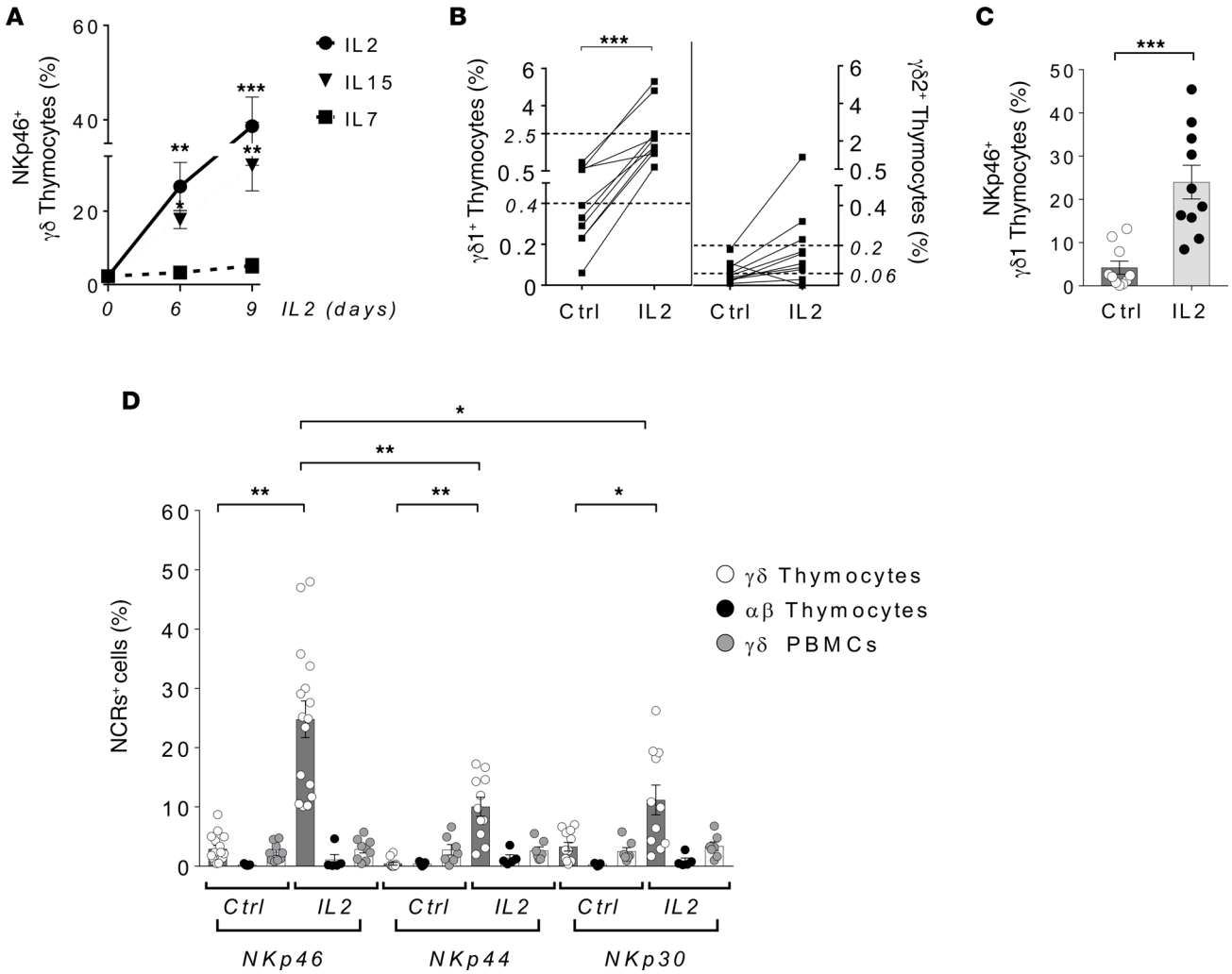

Figure 5. NKp46⁺/Vδ1 T cell expansion following activation of thymocyte precursors with IL-2 or IL-15. (**A**) Summary statistical graphs showing the time course expression of NKp46 in γδ thymocyte precursors ($n \geq 5$) cultured with IL-2 (200 U/mL) or IL-15 (10 ng/mL) or IL-7 (10 ng/mL). (**B**) Summary statistical graphs showing the frequencies of Vδ1 (left graph) and Vδ2 (right graph) thymocytes cultured either in absence (Ctrl) or presence of IL-2 for 6 days ($n = 10$). Data are represented as scattered plots of paired observations. (**C**) Summary statistical graphs showing the frequency of NKp46 expression on Vδ1 thymocytes cultured either in the absence (Ctrl) or in the presence of IL-2 for 6 days ($n = 10$). (**D**) Summary statistical graphs showing NCR expression in γδ and αβ thymocytes, as well as in γδ T cells from PBMCs of healthy donor, cultured either in absence (Ctrl) or in the presence of IL-2 for 6 days ($n \geq 5$). *$P \leq 0.05$; **$P \leq 0.01$; ***$P \leq 0.001$.

distinguishing between IELs and LPLs. We found that the percentages of both total Vδ1 and the NKp46⁺/Vδ1 TIL subsets within CRC tumor mass were significantly lower compared with the frequencies of IELs in disease-free/healthy gut tissue specimens (Figure 7, E and F). Since patients affected by IBD are at higher risk of developing CRC (40), we also evaluated the frequency of both Vδ1 cells and the NKp46⁺/Vδ1 cell subset in patients with ulcerative colitis (UC). Again, the percentages of both of these intestinal lymphocyte populations in the UC gut specimens were significantly lower compared with the frequencies of their IEL counterparts in disease-free/healthy gut tissue specimens (Supplemental Figure 7). Taken together, these data suggest that both inflammatory and tumor microenvironments are associated with escape mechanisms inhibiting either the migration or the in situ expansion of antitumor NKp46⁺/Vδ1 IELs.

Discussion

NKp46 is one of the 3 NCRs originally identified as germline-encoded proteins specifically expressed on circulating NK cells and playing key roles in cancer immune surveillance (41–44). Although NCRs are naturally absent on circulating T cells (17), both NKp46 and NKp44 were previously found to be expressed on human intestinal αβ T IELs of patients affected by celiac disease (45). In this context, a

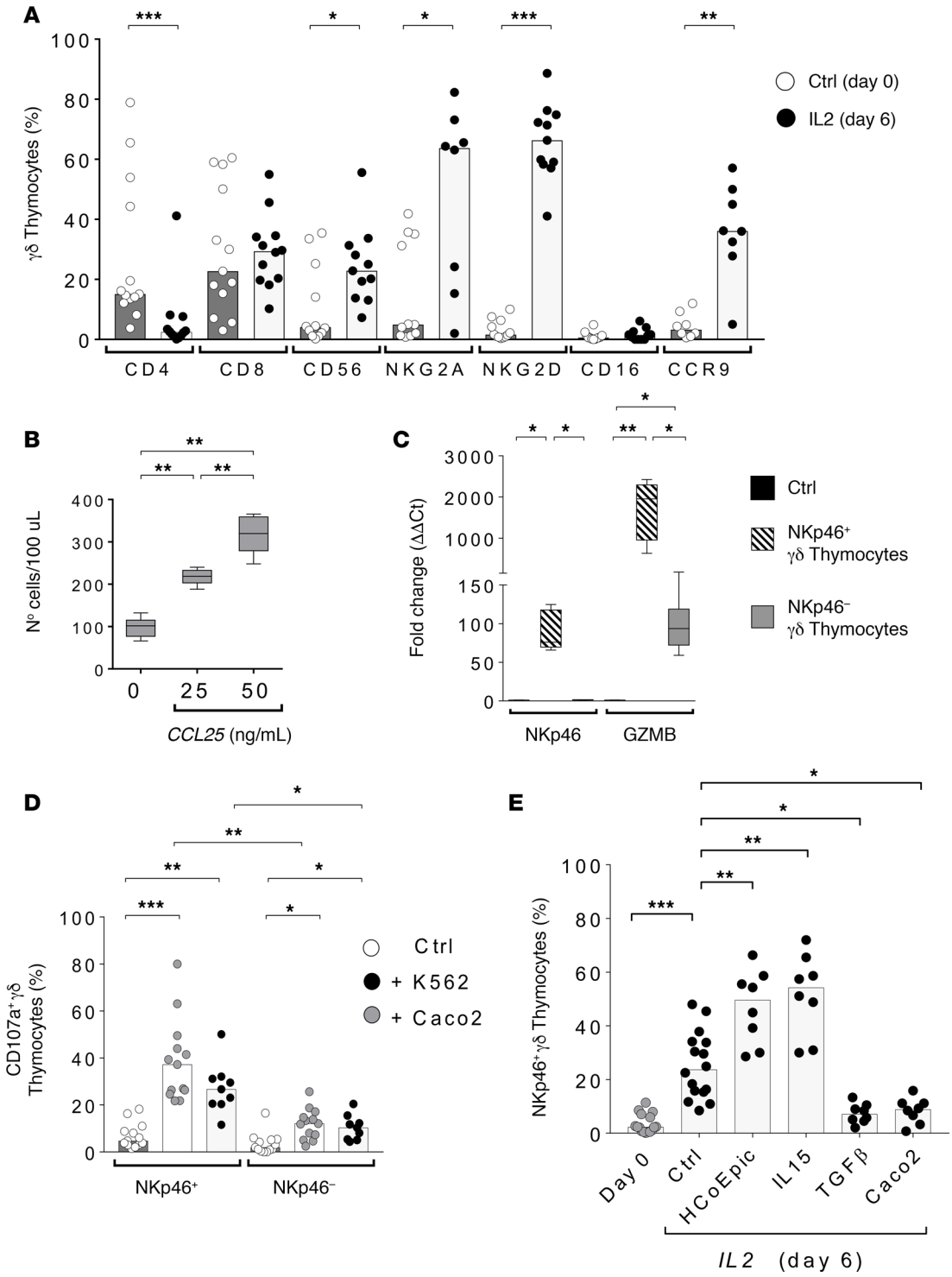

Figure 6. Phenotype and functions of human of NKp46⁺ γδ thymocyte precursors following activations with physiologic and pathologic stimuli. (**A**) Summary statistical graphs showing the expression of CD4, CD8, CD56, NKG2A, NKG2D, CD16, and CCR9 on γδ thymocyte precursors ($n \geq 8$) cultured either in the absence (Ctrl) or presence of IL-2. (**B**) Summary statistical graphs showing the CCL25 dose-dependent chemotaxis of FACS-sorted CCR9⁺/NKp46⁺ Vδ1 T cells generated from thymocyte precursors cultured with IL-2 for 6 days ($n = 8$). (**C**) Summary statistical graphs showing the transcripts levels of GZMB and NKp46 transcripts on freshly FACS-sorted thymocytes (Ctrl) and on NKp46⁺ and NKp46⁻ Vδ1 T cells generated from thymocyte precursors cultured with IL-2 for 6 days ($n = 6$). Results are represented as the fold change ($2^{-\Delta\Delta CT}$) of target gene relative to a Ctrl samples and normalized to housekeeping genes GAPDH and S18. (**D**) Summary statistical graphs showing the expression of CD107a on NKp46⁺ and NKp46⁻ Vδ1 T cells generated from thymocyte precursors cultured with IL-2 for 6 days either in the absence (Ctrl) or in the presence of K562 or Caco2 human tumor target cells ($n \geq 9$). (**E**) Summary statistical graphs showing the NKp46 expression on freshly purified thymocytes (day 0) and on γδ thymocytes cultured with IL-2 for 6 days either in the absence (Ctrl) or in the presence of primary human colonic epithelial cells (HCoEpic) or IL-15, TGF-β, or Caco2 cell lines ($n \geq 8$). $^*P \leq 0.05$; $^{**}P \leq 0.01$; $^{***}P \leq 0.001$.

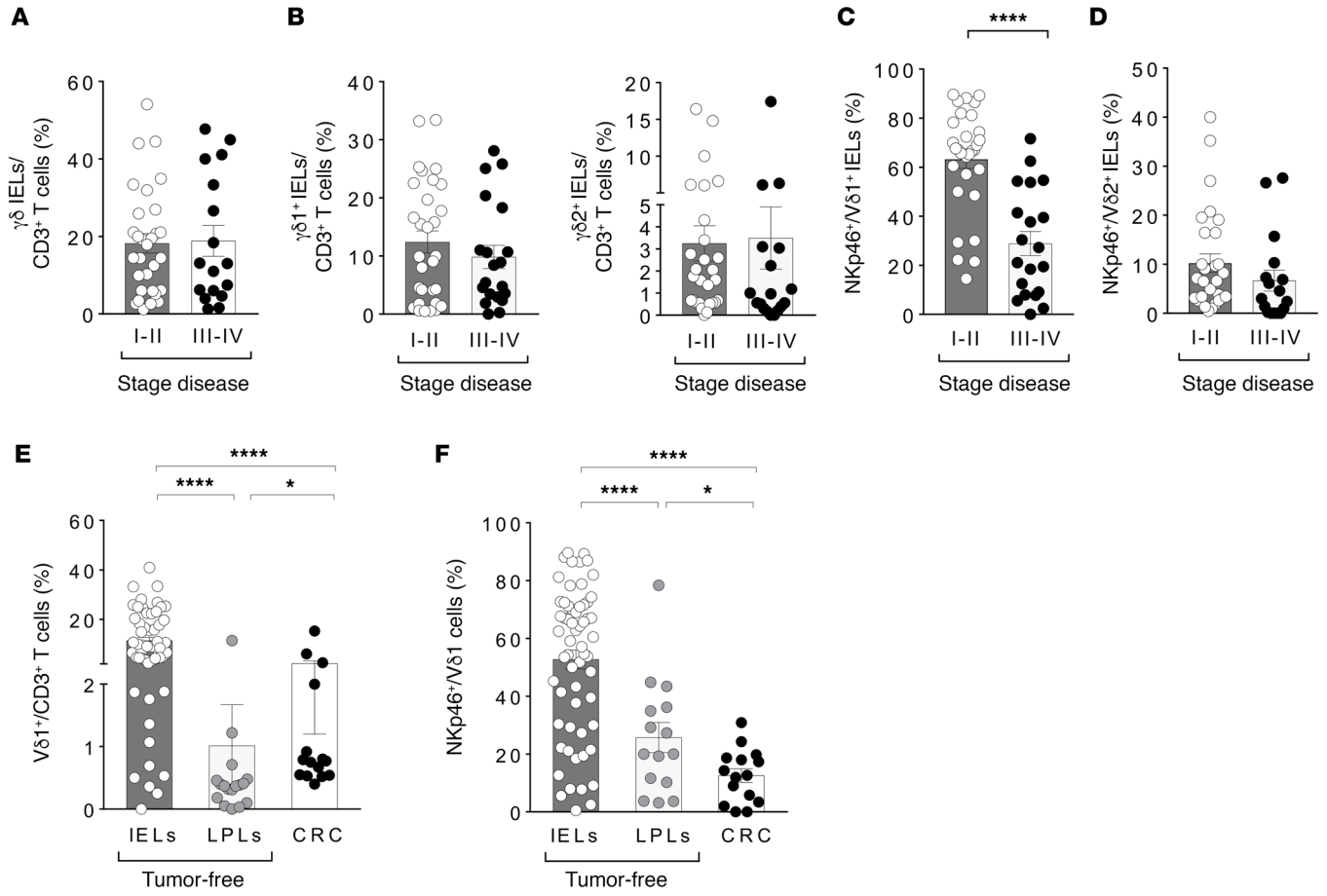

Figure 7. Clinical relevance of the NKp46$^+$/Vδ1 subset in the pathogenesis of CRC. (**A**–**D**) Summary statistical graphs showing the frequencies of total γδ (**A**), Vδ1 and Vδ2 (**B**), NKp46$^+$/Vδ1 (**C**), and NKp46$^+$/Vδ2 (**D**) IEL subsets in healthy intestinal specimens from CRC patients in early (I–II) and late (III–IV) disease stages ($n \geq 17$). (**E** and **F**) Summary statistical graphs showing the frequencies of total Vδ1 cells (**E**) and of the NKp46$^+$/Vδ1 T cell subset (**F**) in both IEL and LPL compartments of healthy/disease-free intestine compared with those of infiltrating gut specimens of colon rectal cancer (CRC) ($n \geq 15$). *$P \leq 0.05$; ****$P \leq 0.0001$.

major role was played by IL-15, a proinflammatory cytokine overexpressed in celiac patients and inducing the expansion of activated NCR$^+$ αβ IELs endowed with potent NK-like and TCR-independent antitumor effector functions (46). However, these cytotoxic NCR$^+$ αβ IELs were highly restricted in their TCR repertoire, likely indicating a previous TCR engagement (47). The present study identifies a subset of Vδ1 cells constitutively expressing high levels of NKp46 and representing the largest γδ IEL subset in healthy human intestine. NKp46$^+$/Vδ1 IELs are not phylogenetically conserved across species (e.g., mice and humans) and are not present in blood and other human tissue compartments highly enriched in γδ T cells. Therefore, they represent a unique population of gut-resident innate-like lymphocytes and a first line of immune-defense against infections and tumors at mucosal interface. This is, to our knowledge, the biggest natural (contrasting to induced) (16) NCR$^+$ T cell subset yet identified.

In this study, we also established a methodology able to induce an NCR$^+$ phenotype on pediatric γδ thymocytes in vitro upon stimulation with IL-15 or IL-2, which are the 2 cytokines playing key roles in boosting the γδ T cell cytotoxicity program (35). This is consistent with a previous report showing that both IL-15 and IL-2 (but not IL-7) induces NCR expression and cytotoxicity on T cells (both αβ and γδ) purified from cord blood (48). Further investigation is needed to understand the kinetics and the mechanisms required in vivo, at the thymus site, to induce the expression of NKp46 on Vδ1 thymocytes, as well as their ability to migrate to gut epithelium.

We previosly reported an inducible expression of NCRs (with NKp30 being the dominant family member) also on circulating γδ T cells from adult donors, a phenomenon occurring selectively on the Vδ1 T cell subset and requiring both IL-15/IL-2 cell activation and TCR engagement (16). NCR$^+$/Vδ1 T cells generated from peripheral blood hold great potential for adoptive cell therapy, as they displayed both in vitro

and in vivo (xenograft models) enhanced cytotoxicity against hematological tumors and potent antiviral activities (49, 50). We show here that the constitutive expression of NKp46 on freshly purified Vδ1 IELs, as well as its induced expression on IL-2/IL-15–stimulated Vδ1 thymocyte precursors, remarkably increase the cytolytic potential of these innate-like lymphocytes against solid (epithelial-derived) tumors, as well.

Taken together, these data demonstrate that the presence of NCRs identifies a subset of highly cytotoxic γδ T cells either normally resident in the human gut epithelium or expanded in vitro from different sources.

The origin and development of IELs is still the subject of debate. A murine model showed that γδ thymocytes follow maturation waves that sequentially populate different tissues, starting with skin at an early embryonic age and followed by tongue, reproductive tract, and intestine at peri- and postnatal days (51). In the gut, there are multiple cellular sources of IL-15, including IECs (37). On the other hand, IL-2 secreted by the neighboring αβ IELs supports the growth of γδ IELs (52). This explains, at least in part, the fact that the intestinal epithelium rather than LP is the preferential natural anatomical location for the newly disclosed NKp46$^+$/γδ IELs. We show here that IL-2 or IL-15 stimulation induces in thymocyte precursors the phenotype and functions of NKp46$^+$/Vδ1 IELs, as well as the expression of CCR9, thus promoting a specific homing of these cells to the IEL compartment (36). In this regard, although IL-2/IL-15–activated γδ thymocyte precursors share several similarities both in phenotype and functions with freshly purified and gut-resident NKp46$^+$/Vδ1 IELs, this latter population lacks the expression of NKG2A in contrast to what we observed in IL-2/IL-15–stimulated thymocytes. The different surface distribution of this iNKR is likely associated with the fact that NKp46$^+$/Vδ1 T cells generated in vitro from thymic precursors do not directly interact with IECs naturally expressing high levels of the nonclassical MHC, Class I, E (HLA-E). This nonclassical MHC-I complex represents the NKG2A natural ligand, whose constitutive high surface level on IECs is a consequence of their chronic stress and antigen challenges occurring at the mucosal interface (53). Therefore, the binding of HLA-E with NKG2A on NKp46$^+$/Vδ1 intestinal IELs might explain its low detectable expression as a mechanism of induced peripheral tolerance under homeostatic conditions and in the presence of alloantigen stimulation. Indeed, NKp46 is involved in the killing of various cancer cells following binding with its natural ligands expressed on cancer cells, a phenomenon also associated with cytoskeletal rearrangement and higher lytic granule polarization to the immune synapse (41, 43, 44, 54, 55). We demonstrate here that the expression of this NCR significantly contributes to the high cytolytic potential of NKp46$^+$/Vδ1 IELs freshly purified from the gut, since its blocking remarkably reduces this effector function. Therefore, while NKp46 expression marks an enhanced cytotoxicity among γδ IELs, other receptors such as NKG2A might represent an immune checkpoint controlling the effector functions of NKp46$^+$/Vδ1 intestinal IELs. Additional studies are required to disclose the mechanisms modulating the immune surveillance thresholds of these newly disclosed subsets of gut-resident innate-like lymphocytes. Taken together, these data indicate that the ontogeny and homeostasis of the NKp46$^+$/Vδ1 IELs depends both on distinctive features of human Vδ1 thymocytes and gut microenvironmental factors.

The clinical relevance of our NKp46$^+$/Vδ1 IELs subset is highlighted by their possible impact in the natural history of CRC. Indeed, our results showed that lower frequencies of NKp46$^+$/Vδ1 IELs in healthy intestinal tissues surrounding the tumor mass correlate with a higher tumor progression toward metastatic diseases. Interestingly, a recent report showed that the NKp46-mediated production of IFN-γ by NK cells is able to control tumor progression and decreases metastasis in vivo via the induced secretion of fibronectin by malignant cells (56). Furthermore, T cells expressing Vδ1 represent the dominant subset among all γδ T cells in CRC patients with an impaired IFN-γ production (21). Our data showed significantly lower frequencies of both CRC intratumoral Vδ1 and NKp46$^+$/Vδ1 T cells compared with those of their counterparts naturally resident in the healthy IE gut compartment. Incubations of IL-2/IL-15–activated thymocyte precursors with Caco2 cells or TGFβ (overexpressed in CRC) (39) greatly inhibited the expansion of NKp46$^+$/Vδ1 T cells. Both these ex vivo and in vitro data suggest that the local tumor microenvironment might facilitate tumor progression by escaping NKp46$^+$/Vδ1 IEL cytotoxicity. A recent study reported that the loss of butyrophilin-like (BTLN) molecule BTLN8 coincides with permanent loss of the specific gut-resident BTLN3/8 reactive Vγ4$^+$/Vδ1 IEL subset upon inflammatory conditions in celiac disease (57). Additional investigations are required to assess if a similar mechanism also contributes to the reduce NKp46$^+$/Vδ1 T cells in human model of cancer like CRC.

In summary, our identification of a gut-resident subset of NKp46$^+$/Vδ1 IELs endowed with enhanced antitumor potential paves the ground for developing novel approaches in the field of immune therapy. Indeed, both the possibility of generating, from thymic precursors in vitro, NKp46$^+$/Vδ1 T cells with

high tropism for the gut and the Delta One T cell protocol (45) — which upregulates NCRs expression on Vδ1 T cells while expanding them to large numbers for adoptive transfer — represent promising and alternative ad hoc strategies for CRC treatment.

Methods

Human specimen processing and cell culture. Healthy intestine tissues were collected from the distal area of the pathological tissue (≥10 cm) and macroscopically free from any disease. In order to obtain intestinal IELs from healthy intestine tissues, gut mucosa was first dissected from the whole tissue and cut in small pieces, washed in wash buffer (WB) prepared with HBSS buffer without Ca_2 and Mg_2 ($HBSS^{-/-}$; Lonza) supplemented with 1% penicillin/streptomycin/amphotericin (P/S/A; Invitrogen), treated with 2 mM of DL-Dithiothreitol (DL-DTT) (Sigma Aldrich) for 15 minutes at room temperature (RT), washed again, and subsequently treated with 2 mM of EDTA (Sigma Aldrich) for 30 minutes at 37°C/5% CO_2. Both cell suspensions were filtered through a 100-μm cell strainer (Thermo Fisher Scientific), and cells were collected by centrifugation (400 *g*, 10 minutes). The remaining tissue was used to isolate LPLs by enzymatic digestion with 0.75 mg/mL of collagenase II (Sigma-Aldrich) for 1 hour at 37°C/5% CO_2. Obtained cells were filtered through a 100-μm cell strainer and collected by centrifugation (400 *g*, 10 minutes). Finally, both IELs and LPLs were isolated using 30/70% Percoll gradient (Sigma-Aldrich) by centrifugation (900 *g* for 20 minutes). Pathological intestine specimens were mechanically minced in small pieces and washed with WB, followed by enzymatic digestion with 1.5 μg/mL of collagenase IV (Invitrogen), 20 μg/mL of hyaluronidase, and 50 μg/mL of DNAase (both from Sigma Aldrich) for 2 hours at 37°C/5% CO_2. Obtained cells were isolated by centrifugation (400 *g*, 10 minutes) and stained for flow cytometry analysis (Supplemental Figure 1, A–C).

Human healthy thymus samples were obtained from children undergoing heart surgery for congenital heart diseases according to current clinical practice. Thymic tissue was cleaned from blood vessels and fat tissue and cut in small pieces. Thymocytes were recovered through mechanical smashing and kept in PBS (Corning) with 1% of P/S, to preserve their viability or were frozen in FBS (Lonza) with 10% of DMSO (Lonza) and stored at –80°C. Thawed thymocytes were cultured in 96-well round-bottom plates at a concentration of 1×10^6 cells/mL in X-VIVO 15 serum-free hematopoietic cell medium supplemented with 5% human AB serum, 1% P/S/A, 1% ultraglutamine, 1% Na pyruvate, and 1% of nonessential amino acid solution (NEAA), all purchased from Lonza. Thymocytes cultured in vitro were stimulated with human recombinant IL-2 (200 U/mL, Miltenyi Biotec) or with IL-15, IL-7, IL-10, IL-12, IL-22, TGF-β, or TSLP, all used at concentration 10 ng/mL and purchased from Peprotech.

Human healthy liver tissues were obtained from patients who underwent hepatectomy for hepatic metastatic disease from CRC. Tissue specimens were collected from the distal area of the pathological tissue (≥4 cm) and macroscopically free from any disease. Liver tissue dissociation was obtained by enzymatic digestion in gentleMACS Dissociator (Miltenyi Biotec) with 2 mg/mL of collagenase D (Roche Diagnostics) for 45 minutes at 37°C/5% CO_2. Cells then were filtered through 100-μm cell strainers and washed in $HBSS^{-/-}$, and lymphocytes were separated using 30/70% Percoll gradient.

Human healthy skin was obtained from patients undergoing abdominoplasty or mastoplasty surgical procedures. Skin specimens were cut in small pieces, and lymphocytes were recuperated by enzymatic digestion with 1.25 U/mL of Dispase II (Roche Diagnostics) initially for 16 hours at 4°C, followed by 30 minutes at 37°C. Solution containing epidermal lymphocytes was filtered through 100-μm cell strainers, and cells were washed in $HBSS^{-/-}$ with5 mM EDTA. Remaining tissue was further digested with 1 mg/mL collagenase D and 1.25 U/mL of Dispase II for 30 minutes at 37°C in order to recover dermis lymphocytes. Cells then were filtered through 100-μm cell strainers and washed in $HBSS^{-/-}$ with 5 mM EDTA, and lymphocytes were separated using 30/70% Percoll gradient.

Human healthy/nonreactive lymph nodes were obtained from patients with Whartin's tumor or hyperplasia of salivary glands. Lymph nodes were mechanically smashed in $HBSS^{-/-}$ through 100-μm cell strainers, and cells were collected by centrifugation (400 *g*, 30 minutes).

Human PBMC were isolated from buffy coats of healthy volunteers (HRH) using Lympholyte Cell Separation density gradient solution (Cederlane Laboratories) according to the manufacturer's instruction.

Primary HCoEpic (catalog 2950; ScienCell Research Laboratories) were cultured on poly-L-lysine (Sigma-Aldrich) following manufacturer's instructions in the specific colonic epithelial cell medium (CoEpiCM, catalog 2951) supplemented with colonic epithelial cell growth supplement (CoEpiCGS, catalog 2952) and 1% P/S/A.

Human leukemia cell line K562 (catalog CCL-243; ATCC) and colon cancer adenocarcinoma Caco2 (catalog HTB37; ATCC), mycoplasma free, were cultured in IMDM (Lonza) or DMEM (Lonza), respectively; both were supplemented with 10% FBS, 1% P/S/A, 1% ultraglutamine. Additional supplements of 1% Na pyruvate and 1% NEAA were added to the Caco2 cell culture medium.

Human SKCO-1 colorectal adenocarcinoma cell line from a metastatic site (ATCC; catalog HTB-39), mycoplasma free, was cultured in EMEM (ATCC) supplemented with 10% FBS and 1% P/S/A.

Mice. Balb-c and C57BL/6 mice were purchased by Charles River Laboratories and maintained under pathogen-free conditions. Small intestine, colon, and spleen specimens were dissected and collected at 4°C in RPMI 1640 (Lonza) medium supplemented with 10% FBS, 1% P/S/A, and 1% ultraglutamine. Cleaned from peyers patches, small intestine and colon tissue were cut in small pieces and treated twice with 1 mM DTT solution (Sigma-Aldrich) for 20 minutes at 37C°/5% CO_2. Cells were then filtered with a 70-μm cell strainer and washed with WB. Total lymphocytes were obtained using 30/70% of Percoll gradient (Sigma-Aldrich) by centrifugation (900 *g* for 20 minutes). Spleen was mechanically smashed in a 100-μm cell strainer (Thermo Fisher Scientific), washed with the WB, and filtered in a 50-μm cell strainer to obtain single-cell suspension of splenocytes.

Flow cytometry. For multiparametric flow cytometry analysis, a standard staining protocol for extracellular markers was used. Briefly, cells were first stained for live/dead discrimination by using Zombie Aqua fixable viability kit (BioLegend) or 7-Aminoactinomycin D (7-ADD; BD Pharmigen). Subsequently, cells were washed with FACS WB ($HBSS^{-/-}$ with 2% of FBS), incubated with Ab mix for 20 minutes in the dark at RT, washed again, and when Zombie Aqua was used, cells were fixed in 1% paraformaldehyde (PFA; Santa Cruz Biotechnology Inc.). Samples were acquired using LSRFortessa cell analyzer system or FACS Canto II (both from BD Biosciences). FACS Aria III cell sorter (BD Biosciences) was used for the specific cell subsets separation and in vitro assays. For sorting experiments, cells were stained with 7-ADD to discriminate dead cells and the appropriate mix of Abs for 20 minutes in the dark at RT. The optimal concentration of all Abs used in the study was defined performing a titration experiment. According to the guidelines for an accurate multicolor flow cytometry analysis, fluorescence minus one (FMO) controls were used for flow cytometry analysis.

For phenotypic analysis, the following specific anti-human mAbs (catalog/clone) were used. From BioLegend, CD3 (317324/SK7; BV650 and 300306/HIT3a; FITC), CD4 (300534/RPAT4; BV570 or 317438; BV605), CD16 (302025/3G8; AF700), CD69 (310938/FN50; BV605), CD103 (350206/BERACT9; PE), γδ TCR (331208/B1; FITC), NKG2D (320812/ID11; PECy7), NKp46 (331914/9E2; BV421), and CCR9 (358906/L053E8; PerCPCy5.5); from BD Biosciences, CD8α (563823/RPAT8; BV780), CD45 (560566/H130; AF700 and 557833/2D1; APCCy7), CD56 (562289/B159; PE-CF594), CD69 (555533/FN50; APC), and NKp30 (563383/P3015; BV711); from Miltenyi Biotec, CD45 (130096609/5B1; APCVio770), KIRs (130103937/REA293; APCVio770 and 130095285/DX27; PerCPCy5.5), Vδ1 (130120440/REA173; PE and 130100542; PEVio770), and NKG2A (130098812/REA111; APC); from eBioscience, CD8β (25527342/5IDI8BEE; PECy7); from Beckman Coulter, Vδ2 (IM1464/IMMU-389; FITC) and NKp44 (PNA66903/Z231; PECy5); and from R&D systems, NKG2C (FAB138C/134591; PerCP).

Mouse γδ T lymphocytes were stained with live/dead discriminating marker 7-ADD and with the specific anti-mouse mix of mAbs: CD3 (555274/17A2; FITC; BD Pharmigen), NKp46 (561169/29A1.4; AF700; BD Pharmigen), and γδ TCR (17571182/eBioGL3; APC; eBioscience).

Cell cytotoxic activity was assessed by CD107a flow cytometry–based assay. Freshly isolated effector IELs or thymocytes were plated in 96-well plates at a concentration 1×10^6 cells/mL in the presence or not of target cells K562 or Caco2 at a ratio of effector/target ratio (E:T) = 1:1 in X-VIVO 15 complete medium and 8 μg/mL of PE-conjugated anti-CD107a Ab (555801/H4A3; BD Biosciences). After 4 hours of incubation at 37°C/5% CO_2, cells were collected, washed in $HBSS^{-/-}$, and stained for extracellular markers as described above. PBMC obtained from healthy donors prestimulated 1 hour with PMA (0.5 μg/mL) and ionomycin (0.1 μg/mL) (both from Sigma-Aldrich) were used as the control of the degranulation assay. For masking experiments, the specific anti-hNKp46 IgM blocking mAb (KL247) was provided by Silvia Parolini (University of Brescia, Brescia, Italy) (58).

Intracellular IFN-γ, TNF-α, and GZMB accumulation was measured by flow cytometry. Freshly isolated IELs were plated in 96-well round-bottom plates at a concentration of 1×10^6 cells /mL with or without target cells K562 at a ratio of E:T = 1:1 and in the presence of 1 μg/mL of Golgi Plug, protein transport inhibitor (BD Biosciences). As a protein transport inhibitor (containing Brefeldin A), Golgi Plug was able

to trap the amounts of newly synthesize (i.e., increased intracellulare levels) GZMB and IFN-γ at the intracellular site in response to activation stimuli. After 4 hours at 37°C/5% CO_2, IELs were collected and washed with $HBSS^{-/-}$, and extracellular staining, as described above, was performed. Subsequently, intracellular staining was done using Cytofix/Cytoperm and Perm/Wash kits (BD Biosciences) according to the manufacturer's instructions and using specific anti-human Abs (BD Biosciences) for TNF-α (559321/Mab11; PE), IFN-γ (564039/B27; BV711), and GZMB (560212/GB11; AF647).

For chemotaxis experiments, viable $CD45^+/CD3^+/\gamma\delta$ $TCR^+/NKp46^+$ IL-2 activated human thymocytes were sorted and plated in X-VIVO 15 complete medium in the basket of the transwell with 8.0 μm large pore (Corning). Human recombinant CCL25 (BioLegend) was added to the bottom of the transwells at different concentrations — 0, 25 and 50 ng/mL — and left 6 hours at 37°C/5% CO_2. After this time, cells were collected and counted by LSRFortessa flow cytometry for quantification.

High-throughput analysis of TRG and TRD repertoires. CDR3 regions of either the γ chain (TRG) or δ chain (TRD) were amplified from flow cytometry-sorted $NKp46^+$ and $NKp46^-$ Vδ1 IELs via a previously described mRNA-based multiplex PCR amplification method (59). PCR amplicons were indexed with the Illumina Nextera Index Kit, purified with Agencourt AMPure beads, equally pooled with 96 samples, and sequenced at the Illumina MiSeq platform (paired-end, 500 cycles, high-output) as recommended by Illumina guidelines, while 20% PhIX was used as a spike-in control. The obtained fastq files of read1 were annotated with MiXCR software (60) using default parameters and further analyzed with the R package TcR (61) and VDJtools (61, 62). For TRD repertoires, only $V\delta1^+$ sequences were processed after MiXCR annotation. Treemaps were generated with the R package treemap. The deposited bio-project number is PRJNA558198

Quantitative PCR. Total RNA of sorted γδ T $NKp46^+$ and $NKp46^-$ IELs/thymocytes was extracted using RNeasy micro-plus columns with RNase-free DNase treatment and RNA carrier (Qiagen) following the manufacturer's instructions. Extracted RNA was used to generate cDNA templates for quantitative PCR (qPCR) using High-Capacity cDNA Reverse Transcription Kit with random primers and RNase inhibitor (Applied Biosystems). A total of 100 ng of total cDNA were preamplified for the specific gene expression using TaqMan mRNA gene assays and TaqMan PreAmp Master Mix (both from Applied Biosystems). qPCR reactions were performed by Real Time AB7900 (Applied Biosystems) with TaqMan Universal PCR Master Mix and the specific TaqMan mRNA gene assays (Applied Biosystems): NCR1 (HS00183683), IL-10 (HS00961622), IL-17A (HS00174383), TGFβ (HS00998133), IL-22 (HS01574154), IFN-γ (HS00989291), GZMB (HS01554355), XCL1 (HS00751481), and housekeeping S18 (HS01026310) and GAPDH (HS02758991). PCR-based detection of mycoplasmal DNA was performed using BioMix (Bioline) and GPO-1 (5′-ACTCCTACGGGAGGCAGCAGT-3′) and MGSO (5′-TGCACCATCTGTCACTCTGTTAACCTC-3′) primers from IDT.

IHC and Immunofluorescence. Formalin-fixed paraffin-embedded liver specimens, previously sectioned with a microtome HM310 Microm (GMI) at 2–4 μm thickness and mounted onto charged glass slides Superfrost (Thermo Fisher Scientific) were stained with H&E using a standard protocol. Briefly, after 2 changes of xylenes, rehydration in an ethanol/water gradient (100%, 90%, 70%), followed by washing in water, slides were stained with in Mayer's Hematoxylin solution (Dako) for 18 minutes, differentiated under running tap water for 10 minutes, and stained with 1% aqueous solution of Eosin Y (Dako) for 8 minutes, followed by 3 washes with 100% ethanol and 3 washes with xylenes. Lastly, H&E-stained slides were mounted with Eukitt (Sigma-Aldrich) and dried prior to imaging by Microscope BX51 (Olympus).

Freshly isolated tissues were fixed with 4% paraformaldehyde for 2 hours and washed and incubated overnight in 30% sucrose. Tissues were then embedded in OCT, frozen in a bath of isopentane cooled on dry ice, and cut in 8 μm–thick sections. Human NKp46 staining was then performed using polyclonal goat anti–human NKp46 (catalog AF1850; R&D Systems; used 20 μg/mL), polyclonal rabbit anti–human CD3 (catalog A0452; Dako; diluted 1:50), and mouse monoclonal anti–human TCR-PAN γδ (COIM1349/IMMU510) (10 μg/mL), followed by the following secondary polyclonal antibodies raised in donkey (Invitrogen): anti–rabbit Alexa488 (catalog A-11008), anti–mouse Alexa594 (catalog A-21203), and anti–goat Alexa647 (catalog A-21447), all used at concentration of 1:1000. Nuclei were counterstained with DAPI (Invitrogen) at concentration of 1:50,000. After staining, slides were dried, mounted with Prolong Gold (Invitrogen), and examined under Zeiss LSM 510 confocal microscope. Image processing was performed with Zeiss LSM and Adobe Photoshop software

Statistics. Statistical analyses were performed using GraphPad Prism version 7. For the comparison of 2 matched groups of samples (specified in the legend) Wilcoxon *t* test was applied or nonpaired Mann-Whitney *U* test was applied. Experiments with more than 2 groups were analyzed by Kruskal-Wallis with Dunn's

post hoc multiple comparisons test. When specified, Pearson's data correlation and R^2 analyses were used. The data are depicted as vertical bars corresponding to mean value ± SEM with scatter dots or as box-and-whisker plots with the median value displayed inside the box and the maximum and minimum values displayed with whiskers. Some graphs are represented as scattered plots of paired observations. $P > 0.05$ was considered not statistically significant (ns). Statistically significant P values were represented with GraphPad (GP) style, $P \leq 0.05$ was considered statistically significant. Flow cytometry data were analyzed by FlowJo software version 9.4 and 9.6 (FlowJo LLC). Flow cytometry data analysis based on t-SNE algorithm were performed using FlowJo 9.6 software.

Study approval. Patient recruitment and sample collection have been performed according to the Declaration of Helsinki. The collection of human samples for research purposes was ethically approved by the IRB of Humanitas Research Hospital (HRH) for blood and gut specimens either free of diseases of affected by CRC or IBDs of patients undergoing surgical gut resection, as well as for healthy skin of patients undergoing plastic surgical procedures (approval 2012/1021), for healthy lymph nodes of patients undergoing the removal of benign head-neck tumors (approval 2010/700), and for healthy liver specimens of patients undergoing resection of CRC metastasis (approval 168/18). We also received IRB approval from the University Hospital of Palermo (UNIPA) for the collection of gut specimens affected by CRC of patients undergoing surgical gut resection (approval 13/2013) and from the IRB of TIGET/San Raffaele Institute for specimens of healthy thymus from pediatric patients undergoing cardiac surgery (approval TIGET07, TCTO-044). All participants or parents with the custody of the child undergoing cardiac surgery were informed about the aims of this research program and signed a detailed informed consent.

Animal experiments adhered to the requirements of the European Commission Directive 86/609/EEC and to the Italian legislation (Decreto Legislativo 116; 27 January 1992). Experiments were approved by the Animal Care and Use Committee from Italian Ministry of Health (approval 158/2011).

Author contributions

JM, FO, EB, AR, BSS, and DM designed and performed experiments. AV, MB, IB, ELP, SM, FD, SV, SD, SDB, MMC, MS, G. Cugini, G. Colombo, EM, MK, and AS provided biological specimens, reagents, and experimental protocols. FSC provided assistance with flow cytometry and cell sorting. PS and MR provided pathologic examination of tissue specimens. IP, SR, and BDL performed TCR repertoire sequencing and analysis. JM, FO, and DM designed the study, analyzed data, and wrote the manuscript. DM directed the study.

Acknowledgments

The authors thank the patients for their generosity and participation in this study and the nurses of the Colon and Rectal Surgery Unit (Humanitas Clinical and Research Center). We thank Matteo Cimino, Matteo Donadon, and Guido Torzilli from Humanitas Clinical and Research Center and Humanitas University for providing specimens of human healthy liver; we thank Genni Enza Marcovecchio from San Raffaele Scientific Institute for providing specimens of healthy human thymus. We thank Kelly Hudspeth, Elena Pontarini, and Manuela Lo Porto from Humanitas Clinical and Research Center for their help in the implementation of experimental protocols and Stefano Mantero from Consiglio Nazionale delle Ricerche for his support in immunochemistry. We also thank Silvia Parolini for anti-NKp46 blocking mAb.

This work was supported by Associazione Italiana per la Ricerca sul Cancro (IG 14687 to DM), the Italian Ministry of Health (Bando Giovani Ricercatori GR2011023477381 to KH and GR-2013-02356522 to AR), intramural research and clinical funding programs of HRH (to DM), and Fondazione Telethon (SR-Tiget F3 core grant to MB) and National Program of CNR Aging Project (to AV).

Address correspondence to: Domenico Mavilio, Unit of Clinical and Experimental Immunology, Department of Medical Biotechnologies and Translational Medicine, University of Milan School of Medicine, Humanitas Clinical and Research Center, Via Alessandro Manzoni, 113, Rozzano (Milan), Italy. Phone: 39.02.8224.5157; Email: domenico.mavilio@unimi.it.

1. Mowat AM, Agace WW. Regional specialization within the intestinal immune system. *Nat Rev Immunol*. 2014;14(10):667–685.
2. Gopalakrishnan V, et al. Gut microbiome modulates response to anti-PD-1 immunotherapy in melanoma patients. *Science*. 2018;359(6371):97–103.
3. Deusch K, Lüling F, Reich K, Classen M, Wagner H, Pfeffer K. A major fraction of human intraepithelial lymphocytes simultaneously expresses the gamma/delta T cell receptor, the CD8 accessory molecule and preferentially uses the V delta 1 gene segment. *Eur J Immunol*. 1991;21(4):1053–1059.
4. Chien YH, Meyer C, Bonneville M. γδ T cells: first line of defense and beyond. *Annu Rev Immunol*. 2014;32:121–155.
5. Nielsen MM, Witherden DA, Havran WL. γδ T cells in homeostasis and host defence of epithelial barrier tissues. *Nat Rev Immunol*. 2017;17(12):733–745.
6. Roberts SJ, et al. T-cell alpha beta + and gamma delta + deficient mice display abnormal but distinct phenotypes toward a natural, widespread infection of the intestinal epithelium. *Proc Natl Acad Sci USA*. 1996;93(21):11774–11779.
7. Fujihashi K, et al. gammadelta T cells regulate mucosally induced tolerance in a dose-dependent fashion. *Int Immunol*. 1999;11(12):1907–1916.
8. Vantourout P, Hayday A. Six-of-the-best: unique contributions of γδ T cells to immunology. *Nat Rev Immunol*. 2013;13(2):88–100.
9. Bottino C, et al. Two subsets of human T lymphocytes expressing gamma/delta antigen receptor are identifiable by monoclonal antibodies directed to two distinct molecular forms of the receptor. *J Exp Med*. 1988;168(2):491–505.
10. Scotet E, et al. Tumor recognition following Vgamma9Vdelta2 T cell receptor interactions with a surface F1-ATPase-related structure and apolipoprotein A-I. *Immunity*. 2005;22(1):71–80.
11. Tanaka Y, Morita CT, Tanaka Y, Nieves E, Brenner MB, Bloom BR. Natural and synthetic non-peptide antigens recognized by human gamma delta T cells. *Nature*. 1995;375(6527):155–158.
12. Gober HJ, Kistowska M, Angman L, Jenö P, Mori L, De Libero G. Human T cell receptor gammadelta cells recognize endogenous mevalonate metabolites in tumor cells. *J Exp Med*. 2003;197(2):163–168.
13. Zou C, Zhao P, Xiao Z, Han X, Fu F, Fu L. γδ T cells in cancer immunotherapy. *Oncotarget*. 2017;8(5):8900–8909.
14. Silva-Santos B, Serre K, Norell H. γδ T cells in cancer. *Nat Rev Immunol*. 2015;15(11):683–691.
15. Correia DV, Lopes A, Silva-Santos B. Tumor cell recognition by γδ T lymphocytes: T-cell receptor vs. NK-cell receptors. *Oncoimmunology*. 2013;2(1):e22892.
16. Correia DV, Fogli M, Hudspeth K, da Silva MG, Mavilio D, Silva-Santos B. Differentiation of human peripheral blood Vδ1+ T cells expressing the natural cytotoxicity receptor NKp30 for recognition of lymphoid leukemia cells. *Blood*. 2011;118(4):992–1001.
17. Hudspeth K, Silva-Santos B, Mavilio D. Natural cytotoxicity receptors: broader expression patterns and functions in innate and adaptive immune cells. *Front Immunol*. 2013;4:69.
18. Wu D, Wu P, Qiu F, Wei Q, Huang J. Human γδT-cell subsets and their involvement in tumor immunity. *Cell Mol Immunol*. 2017;14(3):245–253.
19. Pang DJ, Neves JF, Sumaria N, Pennington DJ. Understanding the complexity of γδ T-cell subsets in mouse and human. *Immunology*. 2012;136(3):283–290.
20. Gentles AJ, et al. The prognostic landscape of genes and infiltrating immune cells across human cancers. *Nat Med*. 2015;21(8):938–945.
21. Meraviglia S, et al. Distinctive features of tumor-infiltrating γδ T lymphocytes in human colorectal cancer. *Oncoimmunology*. 2017;6(10):e1347742.
22. Gibbons DL, Spencer J. Mouse and human intestinal immunity: same ballpark, different players; different rules, same score. *Mucosal Immunol*. 2011;4(2):148–157.
23. Sathaliyawala T, et al. Distribution and compartmentalization of human circulating and tissue-resident memory T cell subsets. *Immunity*. 2013;38(1):187–197.
24. Cepek KL, et al. Adhesion between epithelial cells and T lymphocytes mediated by E-cadherin and the alpha E beta 7 integrin. *Nature*. 1994;372(6502):190–193.
25. Hayday A, Theodoridis E, Ramsburg E, Shires J. Intraepithelial lymphocytes: exploring the Third Way in immunology. *Nat Immunol*. 2001;2(11):997–1003.
26. Kadivar M, Petersson J, Svensson L, Marsal J. CD8αβ+ γδ T Cells: A Novel T Cell Subset with a Potential Role in Inflammatory Bowel Disease. *J Immunol*. 2016;197(12):4584–4592.
27. Hunter S, et al. Human liver infiltrating γδ T cells are composed of clonally expanded circulating and tissue-resident populations. *J Hepatol*. 2018;69(3):654–665.
28. Hudspeth K, et al. Human liver-resident CD56(bright)/CD16(neg) NK cells are retained within hepatic sinusoids via the engagement of CCR5 and CXCR6 pathways. *J Autoimmun*. 2016;66:40–50.
29. Tomasello E, et al. Mapping of NKp46(+) Cells in Healthy Human Lymphoid and Non-Lymphoid Tissues. *Front Immunol*. 2012;3:344.
30. Di Lorenzo B, Ravens S, Silva-Santos B. High-throughput analysis of the human thymic Vδ1$^+$ T cell receptor repertoire. *Sci Data*. 2019;6(1):115.
31. Bamias G, Arseneau KO, Cominelli F. Cytokines and mucosal immunity. *Curr Opin Gastroenterol*. 2014;30(6):547–552.
32. Boismenu R, Feng L, Xia YY, Chang JC, Havran WL. Chemokine expression by intraepithelial gamma delta T cells. Implications for the recruitment of inflammatory cells to damaged epithelia. *J Immunol*. 1996;157(3):985–992.
33. Gomes AQ, et al. Identification of a panel of ten cell surface protein antigens associated with immunotargeting of leukemias and lymphomas by peripheral blood gammadelta T cells. *Haematologica*. 2010;95(8):1397–1404.
34. Van de Walle I, et al. Specific Notch receptor-ligand interactions control human TCR-αβ/γδ development by inducing differential Notch signal strength. *J Exp Med*. 2013;210(4):683–697.
35. Ribot JC, Ribeiro ST, Correia DV, Sousa AE, Silva-Santos B. Human γδ thymocytes are functionally immature and differentiate into cytotoxic type 1 effector T cells upon IL-2/IL-15 signaling. *J Immunol*. 2014;192(5):2237–2243.
36. Kabelitz D, Wesch D. Features and functions of gamma delta T lymphocytes: focus on chemokines and their receptors. *Crit Rev Immunol*. 2003;23(5-6):339–370.
37. Qiu Y, Wang W, Xiao W, Yang H. Role of the intestinal cytokine microenvironment in shaping the intraepithelial lymphocyte

repertoire. *J Leukoc Biol*. 2015;97(5):849–857.
38. Ziegler SF, Liu YJ. Thymic stromal lymphopoietin in normal and pathogenic T cell development and function. *Nat Immunol*. 2006;7(7):709–714.
39. Tauriello DVF, Batlle E. Targeting the Microenvironment in Advanced Colorectal Cancer. *Trends Cancer*. 2016;2(9):495–504.
40. Janakiram NB, Rao CV. The role of inflammation in colon cancer. *Adv Exp Med Biol*. 2014;816:25–52.
41. Glasner A, et al. Recognition and prevention of tumor metastasis by the NK receptor NKp46/NCR1. *J Immunol*. 2012;188(6):2509–2515.
42. Moretta A, Bottino C, Mingari MC, Biassoni R, Moretta L. What is a natural killer cell? *Nat Immunol*. 2002;3(1):6–8.
43. Lakshmikanth T, et al. NCRs and DNAM-1 mediate NK cell recognition and lysis of human and mouse melanoma cell lines in vitro and in vivo. *J Clin Invest*. 2009;119(5):1251–1263.
44. Halfteck GG, Elboim M, Gur C, Achdout H, Ghadially H, Mandelboim O. Enhanced in vivo growth of lymphoma tumors in the absence of the NK-activating receptor NKp46/NCR1. *J Immunol*. 2009;182(4):2221–2230.
45. Meresse B, et al. Reprogramming of CTLs into natural killer-like cells in celiac disease. *J Exp Med*. 2006;203(5):1343–1355.
46. Meresse B, et al. Coordinated induction by IL15 of a TCR-independent NKG2D signaling pathway converts CTL into lymphokine-activated killer cells in celiac disease. *Immunity*. 2004;21(3):357–366.
47. Meresse B, et al. Reprogramming of CTLs into natural killer-like cells in celiac disease. *J Exp Med*. 2006;203(5):1343–1355.
48. Tang Q, et al. Umbilical cord blood T cells express multiple natural cytotoxicity receptors after IL-15 stimulation, but only NKp30 is functional. *J Immunol*. 2008;181(7):4507–4515.
49. Almeida AR, et al. Delta One T Cells for Immunotherapy of Chronic Lymphocytic Leukemia: Clinical-Grade Expansion/Differentiation and Preclinical Proof of Concept. *Clin Cancer Res*. 2016;22(23):5795–5804.
50. Hudspeth K, et al. Engagement of NKp30 on Vδ1 T cells induces the production of CCL3, CCL4, and CCL5 and suppresses HIV-1 replication. *Blood*. 2012;119(17):4013–4016.
51. Allison JP, et al. Gamma delta T cells in murine epithelia: origin, repertoire, and function. *Adv Exp Med Biol*. 1991;292:63–69.
52. Chu CL, Chen SS, Wu TS, Kuo SC, Liao NS. Differential effects of IL-2 and IL-15 on the death and survival of activated TCR gamma delta+ intestinal intraepithelial lymphocytes. *J Immunol*. 1999;162(4):1896–1903.
53. Perera L, et al. Expression of nonclassical class I molecules by intestinal epithelial cells. *Inflamm Bowel Dis*. 2007;13(3):298–307.
54. Bloushtain N, et al. Membrane-associated heparan sulfate proteoglycans are involved in the recognition of cellular targets by NKp30 and NKp46. *J Immunol*. 2004;173(4):2392–2401.
55. Hadad U, Thauland TJ, Martinez OM, Butte MJ, Porgador A, Krams SM. NKp46 Clusters at the Immune Synapse and Regulates NK Cell Polarization. *Front Immunol*. 2015;6:495.
56. Glasner A, et al. NKp46 Receptor-Mediated Interferon-γ Production by Natural Killer Cells Increases Fibronectin 1 to Alter Tumor Architecture and Control Metastasis. *Immunity*. 2018;48(1):107–119.e4.
57. Mayassi T, et al. Chronic Inflammation Permanently Reshapes Tissue-Resident Immunity in Celiac Disease. *Cell*. 2019;176(5):967–981.e19.
58. Pende D, et al. Identification and molecular characterization of NKp30, a novel triggering receptor involved in natural cytotoxicity mediated by human natural killer cells. *J Exp Med*. 1999;190(10):1505–1516.
59. Ravens S, et al. Human γδ T cells are quickly reconstituted after stem-cell transplantation and show adaptive clonal expansion in response to viral infection. *Nat Immunol*. 2017;18(4):393–401.
60. Bolotin DA, et al. MiXCR: software for comprehensive adaptive immunity profiling. *Nat Methods*. 2015;12(5):380–381.
61. Nazarov VI, et al. tcR: an R package for T cell receptor repertoire advanced data analysis. *BMC Bioinformatics*. 2015;16:175.
62. Shugay M, et al. VDJtools: Unifying Post-analysis of T Cell Receptor Repertoires. *PLoS Comput Biol*. 2015;11(11):e1004503.